ROYAL SOCIETY
OF CHEMISTRY

Check for updates

Metal oxide heterostructure towards gas sensing of trimethylamine: recent progress and challenges

Kimiya Karimi,[a] Amin Foroozandeh,[a] Hossein Salar Amoli*[a]
and Mohammad Hasanzadeh [ID] *[b]

Gas sensors based on metal oxide heterostructures (MOHs) are popular due to their low cost, sensitivity, and eco-friendly production. MOHs significantly improve trimethylamine (TMA) detection sensor performance in different food analyses. These improvements stem from their capability to enhance reaction efficiency, elevate adsorption potential, and create a region with reduced charge carriers. The synergistic effects of these factors collectively enhance the sensor's sensitivity, selectivity, and signal transmission efficiency. However, challenges still need to be addressed, including potential material migration at the junctions, manufacturing process reproducibility, and sensing layer stability. This review highlighted the significant role of MOHs in chemical sensing, with a particular emphasis on their application in detecting TMA for food quality analysis. This review explored the growth and interfacial characteristics of MOHs-based sensors of TMA, aiming to bridge the gap between laboratory research and practical applications. Additionally, we surveyed the mechanisms and impact of different MOHs on the performance of TMA sensors in food analysis, providing insights into their effectiveness and real-world implementation. Furthermore, the role of microfluidic sensors and the significance of artificial intelligence were explored to improve the significant factors in detecting toxic gases and monitoring environmental health quality. Integrating AI and microfluidic technologies could enhance real-time calibration and detection accuracy, addressing these limitations. Future work could be focused on improving sensor design and environmental resilience to ensure the broader use of MOH sensors in food safety and environmental monitoring.

1. Introduction

The food industry plays a vital role in shaping the global economy, public health, and cultural practices, serving as an essential sector that provides sustenance and influences various aspects of society.[1] From the production and processing of food to its distribution and consumption, this industry has a significant role in science and innovation development.[2–5] Furthermore, the food industry is responsible for upholding stringent safety and quality standards across the supply chain, ensuring consumer health and compliance with regulatory requirements.[6] Strict regulations and quality control measures are implemented to prevent contamination, spoilage, and the spread of diseases. Additionally, the industry plays a vital role in promoting healthy eating habits by providing consumers with a diverse range of food options and nutritional information.[7–9] This helps combat issues such as malnutrition, obesity, and diet-related diseases. One of the most important types of food is

meat, including red meat, poultry, and fish, which are rich in nutrients such as protein, fat and minerals.[10–12]

More than 20 percent of primary meat production in North America is lost. In fact, this trend can be attributed to waste in the supply chain.[13] In Canada, the financial burden of food waste surpasses $31 billion annually and escalates beyond $100 billion when factoring in related costs like energy and water consumption.[14] Comparable patterns are observed in other industrialized nations. This significant level of food waste also presents serious environmental concerns. The Food and Agriculture Organization of the United Nations reported that the global carbon footprint attributed to food waste exceeds 4.4 Gt CO_2 annually, with meat spoilage accounting for more than 20% of this impact.[15]

In addition, foodborne disease is prevalent in the world, and food freshness, quality, and flavor can significantly influence people's inclination to consume.[16,17] Aroma and taste are essential indexes of food flavor and freshness, which impact the overall food assessment and consumers' purchasing behavior.[18,19] With improper storage or too long storage time, food will spoil with unpleasant vapors, such as TMA and hydrogen sulfide gas. Released from deteriorated types of food, TMA is a hazardous, volatile organic compound (VOC) that has

[a]Department of Chemistry, Amirkabir University of Technology, Tehran, Iran. E-mail: h.salaramoli@aut.ac.ir

[b]Pharmaceutical Analysis Research Center, Tabriz University of Medical Sciences, Tabriz, Iran. E-mail: hasanzadehm@tbzmed.ac.ir

harmful results on human health.[20–22] Prolonged human exposure to elevated levels of TMA can lead to various adverse health effects, including dyspnea, headaches, pulmonary edema, nausea, and irritation of the upper respiratory tract. As a precautionary measure, the National Institute for Occupational Safety and Health (NIOSH) in the USA has established an exposure limit of 10 ppm over a 10-hour period to minimize health risks.[23,24]

Various analytical techniques have been extensively employed for the detection of TMA, including high-performance liquid chromatography (HPLC), gas chromatography-mass spectrometry (GC-MS), and ion mobility spectrometry (IMS). These methods offer high sensitivity and accuracy, making them effective tools for monitoring TMA levels in different applications.[25,26] These characterization methods often necessitate high-cost, sophisticated instruments, specialized expertise, intricate operational protocols, and extensive sample preparation, making them impractical for real-time food freshness assessment.[20] Research highlights the evolution of sensors from basic detection devices to advanced, high-performance systems with enhanced flexibility, wearability, nanoplasmonic properties, stretchability, and fatigue resistance. These modern sensors exhibit superior temperature tolerance and are increasingly integrated into large-scale applications, including the Internet of Things (IoT) and traceability systems, significantly improving real-time monitoring and data collection capabilities.[27–30]

The GS has been established for decades to gain rapid, accurate, operation-friendly, and even online detection techniques for odor quality of nutrition substances.[31,32] Recent research has shown that GSs are mainly designed according to sensing materials and transducer devices.[33] Among a type of gas-sensitive materials, MOHs, including WO_3, ZnO, MoO_3, α-Fe_2O_3, SnO_2, and CeO_2, have been widely considered.[34–40] Today, many scientists and researchers consider the use of MO in various fields, especially sensor fabricating, to be a useful

endeavor. As illustrated in Fig. 1, the global market for gas sensors (GSs) has shown a consistent growth trend from 2020 to 2024, with continued expansion projected through 2030. The demand is driven by emerging applications in environmental monitoring, industrial automation, healthcare, and particularly in food quality and safety. Notably, the Asia Pacific region leads the market, followed by North America and Europe, indicating both technological and regional dynamics in sensor adoption. This trajectory underscores the increasing importance of GS technologies, including advanced architectures such as metal oxide heterostructures (MOHs).[41] They are widely regarded as cost-effective materials for GSs, offering several benefits, including exceptional sensitivity, rapid response and recovery, low detection limits, and affordability in fabrication. Additionally, they stand out for their ease of manufacturing, straightforward measurement processes, and long-lasting functionality in comparison to other SC materials.[42–45] The metal oxide semiconductor (MOS) are widely regarded as cost-effective materials for GS applications. They offer several advantages, including exceptional sensitivity, rapid response and recovery times, low detection limits, and affordability in manufacturing. Additionally, their straightforward fabrication process, ease of measurement, and long-term functional stability make them superior to many other SC-based sensors.[20,46,47]

Since the 1970s, they have been designed as porous polycrystalline films, serving as standard sensor materials for conductometric GSs in the market.[48] HS nanomaterials (NMs) exhibit outstanding electrochemical properties, including improved conductivity, remarkable charge storage capacity, extended cycle life, and enhanced energy and power output. These superior properties arise from the synergistic interaction among their components, making them highly sought-after for resistive sensor design. The incorporation of heterostructure (HSs) into heterojunctions (HJs) enhances sensing capabilities by leveraging catalytic activity, increasing adsorption efficiency, and facilitating the formation of a depletion layer.[49–51] HSs are
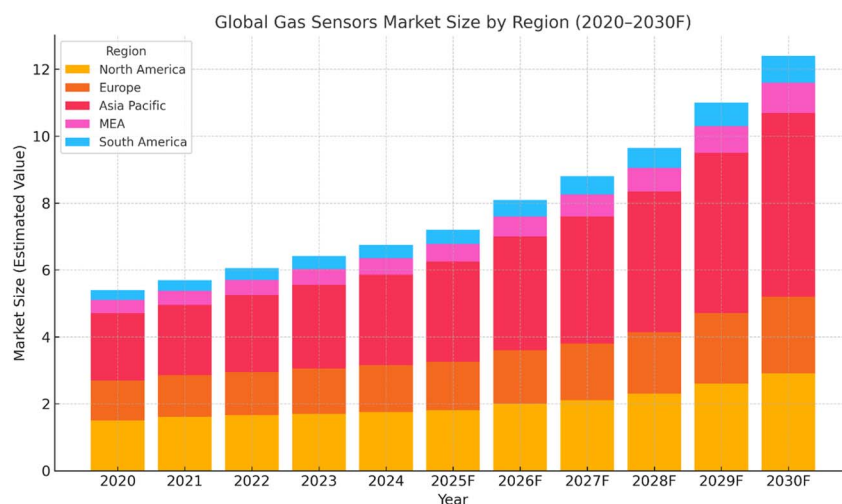

Fig. 1 Global GS market size by region and value (2020–2030F). Actual values up to 2024 and projected values from 2025 to 2030. TechSci Research, GSs Market Report, 2024.

generally categorized into mixed, bi- or multi-layered, decorated, core–shell, and branched configurations.[52] Given the rapid advancements in GSs for food quality assessment, this review specifically focuses on MOH-based sensors used in the detection of trimethylamine (TMA), a key volatile compound associated with food spoilage. While several comprehensive reviews have been published on general MOH GS technologies,[90] our study provides a TMA-centered perspective by systematically comparing the structural, compositional, and morphological characteristics of MOHs and their specific impact on TMA sensing performance.[49,53–55]

2. Historical review of TMA sensors

In recent years, applying GSs to evaluate food quality has become a new approach, and it has been considered worldwide.[56] Some recent studies in Table 1 showcase the TMA sensing performance of various MOs. According to Song et al., incorporating noble metals (NbMs) into the sensor material is considered an effective strategy for enhancing GS performance.[57] Therefore, a new GS material was prepared to detect TMA gas by decorating Au nanoparticles (NPs) on WO_3 nanorods (NRs). GS tests confirmed that the maximum response of the Au@WO_3 sensor is 76.4 at a functional temperature of 280 °C for 100 ppm TMA. Also, the short response/recovery time (6/7 s) in this type of sensor was one of its remarkable features in the detection of TMA gas. In another study by Lee et al.,[58] electrospinning and a deposition method realized a flexible TMA sensor based on In_2O_3 nanofibers (NFs). The sensor demonstrated the ability to detect TMA gas concentrations as low as 1 ppm at 80 °C, with a response value of 3.8.

Additionally, it exhibited rapid response (6 s) and recovery times (10 s).[58] Both studies emphasize the importance of fabrication techniques and material selection in improving TMA sensor sensitivity, response time, and stability. While Au@WO_3 sensors offer high performance at elevated temperatures, In_2O_3 NFs provide a more flexible and lower-temperature option. The use of NbMs and novel nanostructures (NSs) not only improves the detection limits but also contributes to enhanced sensor speed, which is critical for real-time applications. However, the performance stability of these sensors over extended use, particularly in real-world conditions, remains a challenge that requires further investigation. In another study, Rodrigues et al. synthesized Co-doped ZnO NSs (5% and 15%) using a hydrothermal method. The 15% Co-doped sample showed the highest response (86.1%) to 50 ppm TMA at 100 °C, with fast response (19.4 s) and recovery (15.5 s) times. The sensor also exhibited high selectivity toward TMA over various amines and maintained stable performance over a 70-day reproducibility test.[59] In a study by Yun et al., porous In_2O_3 nanoparticles decorated with varying concentrations of CuO (6.7–28.4 at%) were synthesized via a microwave-assisted hydrazine reduction method for TMA GS. The optimal sensor (CuO/In_2O_3), with 23.8 at%, exhibited a response of 5.7 to 2.5 ppm TMA at 325 °C, approximately 2.8 times higher than that of pristine In_2O_3. The enhanced sensing performance was attributed to the p–n HJ formation between CuO and In_2O_3 and the catalytic activity of CuO.[50] A highly sensitive room-temperature TMA sensor was fabricated by integrating MoO_3 nanofibers with layered $Ti_3C_2T_x$ MXene, as reported by Ma et al. The composite exhibited a strong response of 4.0 to 2 ppm TMA, with fast response and recovery times of 10 s and 7 s, respectively. These properties were attributed to the formation of a p–n HJ, high surface area, and abundant active sites that enhanced gas adsorption and charge transfer. The sensor also demonstrated a low detection limit and excellent stability, making it a promising candidate for TMA detection in exhaled breath diagnostics.[60] Hu et al. reported a high-performance

Table 1 TMA sensing performance of various MOs

Morphology	Composition	TMA (ppm)	Temperature (°C)	Synthesis route	Ref.
Nanocomposite	Au@WO_3	100	280	Hydrothermal	57
Nanocomposite	Au/WO_3	25	300	Solvothermal	68
NF	In_2O_3	1	80	Electrospinning	58
Hierarchical architectures	α-Fe_2O_3	100	260	Solvothermal	69
Membrane nanotubes (NTs)	TiO_2	40–400	80	Electrochemical anodization	70
Nanoplates	MoO_3	5	300	Solution base	35
NR	Pd–ZnO	5–5.5	300	Simple wet-chemical	71
Nanocomposite	SnO_2–ZnO	1–500	330	Hydrothermal	20
Nanocomposite	Au@MoO_3	5	280	Hydrothermal	23
Nanowires (NWs)	Cr_2O_3–ZnO	5	400	Thermal evaporation	72
NF	ZnO–In_2O_3	5	300–450	Electrospinning	58
NRs	α-Fe_2O_3/TiO_2	50	250	Electrospinning	73
Nano-materials	CdO–Fe_2O_3	1000	230	Co-precipitation	74
Thin films	Al_2O_3, TiO_2, and V_2O_5-doped ZnO	2	300	Sputtering	75
Nanocomposite	NiO–In_2O_3	10	200	Hydrothermal	76
NRs	1-$NiMoO_4$/MoO_3	0.1–10	200	Simple two-step solvothermal	77
Microspheres	$ZnFe_2O_4$/ZnO	31.5–100	240	Hydrothermal	78
Nanocages	Co_3O_4/ZnO	0.013–50	190	Thermal decomposition (assemble template)	79

TMA GS based on a hollow flower-like NiO structure co-doped with Sn and W, synthesized *via* a simple hydrothermal approach using a metal–organic framework precursor. The sensor exhibited an impressive response of 95 to 100 ppm TMA—approximately 63 times higher than that of undoped NiO nanoflowers. It also demonstrated a ppb-level detection limit, with a notable response of 1.5 to just 0.1 ppm TMA. The superior sensing performance was attributed to the synergistic effects of high initial resistance (R_a), abundant oxygen vacancies, the unique hollow spherical morphology, and an elevated Ni^{3+}/Ni^{2+} ratio in the doped NiO NS.[61] Recent studies have extensively focused on enhancing the selectivity and sensitivity of TMA GSs through heterostructure engineering, surface functionalization, and hybrid nanomaterials. Among them, the work by Meng's team introduced a $NiMoO_4$-functionalized MoO_3 heterostructure that demonstrated remarkable sensitivity and ultra-low detection limits. Their optimized 7% $NiMoO_4$/MoO_3 sensor responded strongly to 0.1 ppm TMA at 200 °C, with a theoretical detection limit of 2.48 ppb. This improvement is attributed to the formation of p–n heterojunctions, enhanced interfacial charge transfer, and the high surface area of the nanosheet structure.[62]

In a parallel effort, Yang reported the development of hollow In_2O_3 nanotubes derived from metal–organic frameworks and surface-modified with RuO_2. The 1.5 wt% RuO_2–In_2O_3 sensor exhibited a record-high response ($R_a/R_g = 338$) to 100 ppm TMA, outperforming pristine In_2O_3 by more than 30-fold. With a response time of just 3 s and a low detection threshold of 50 ppb, this sensor benefits from both chemical and electronic sensitization effects of RuO_2 and the structural advantages of the nanotube architecture.[63]

Moreover, Sui and co-workers demonstrated that MoO_3/V_2O_5 nanocomposites synthesized *via* hydrothermal methods could detect TMA at room temperature with excellent performance. Their composite sensor exhibited a response of 11.37% to 20 ppb TMA—significantly higher than pure MoO_3 or V_2O_5 components. Density functional theory simulations further confirmed the synergistic role of the n–n heterojunction in enhancing the adsorption and sensing capability. The sensor's successful detection of TMA in simulated exhaled breath underlines its promise for non-invasive biomedical diagnostics.[64] Similarly, Ji developed a novel flower-like Co_3O_4/In_2O_3 p–n heterostructure sensor, which not only reduced the operating temperature by 50 °C compared to pure In_2O_3 but also achieved a detection limit down to 1 ppm TMA. The enhanced performance is ascribed to the catalytic effect of Co_3O_4 and the optimized charge separation enabled by the heterojunction interface. This work provides a deeper understanding of the structural and electronic factors governing GS.[65] Similarly, Xie explored a hybrid approach by integrating one-dimensional In_2O_3 nanofibers with two-dimensional $Ti_3C_2T_X$ MXene. The resulting composite sensor exhibited a rapid response/recovery time (4/3 s) and a response value of 12.44 to 50 ppm TMA at 120 °C, which is more than twice that of pristine In_2O_3. The improved performance is attributed to the large surface area and synergistic effect of the 1D/2D interface and the formation of p–n heterojunctions, offering a new avenue for the design of advanced hybrid GSs.[66] Finally, building upon these innovative strategies, Wang and colleagues synthesized Co_3O_4-modified WO_3 microspheres *via* a straightforward hydrothermal route using ZIF-67 as a sacrificial template. The resulting hybrid material exhibited outstanding gas-sensing properties toward TMA. Notably, the WO_3/Co_3O_4-based sensor achieved a high response of 198 to 100 ppm TMA at 285 °C, alongside a fast response/recovery time (11.7/2.1 s), excellent selectivity, long-term operational stability, and a low detection limit of 0.17 ppm. The remarkable performance is attributed to several synergistic factors: the large surface area facilitated by the microspherical morphology, the p–n heterojunction formed between WO_3 and Co_3O_4, which modulates the resistance efficiently upon gas exposure, and the inherent catalytic activity of Co_3O_4 that accelerates the redox reactions at the sensing interface. This study further confirms the vital role of compositional tuning and heterostructure engineering in advancing the field of high-performance TMA GSs.[67] Collectively, these advancements underscore the critical role of heterostructure design, surface modification, and dimensional hybridization in overcoming long-standing challenges such as low sensitivity, high humidity interference, and poor selectivity. These approaches pave the way for the development of next-generation TMA sensors tailored for applications ranging from food safety to non-invasive medical diagnostics.

This review focuses on recent advancements in the design, fabrication, and application of MOHs for the detection of TMA, a VOC of significant importance in food safety, environmental monitoring, and medical diagnostics. The synergistic effects between different MOs in HSs are explored, highlighting how they improve GS performance through mechanisms such as enhanced charge transfer, catalytic activity, and surface area. Key strategies for tailoring HS properties, including doping, morphology control, and interface engineering, are discussed in detail. Furthermore, the review addresses current challenges, such as achieving high selectivity in complex gas environments, improving long-term stability, and scaling up for practical applications. Finally, future research directions are proposed to overcome these limitations and unlock the full potential of MOHs for TMA sensing. This comprehensive overview aims to guide researchers toward innovative solutions in the field of GSs and monitoring of TMA as a VOC.

3. Classification of HS

HJs play a critical role in enhancing the GS performance of MO-based sensors, especially for electron-donating analytes such as TMA. The formation of junctions between two semiconductor (SC) materials (*e.g.*, p–n, n–n, or p–p) leads to built-in electric fields and charge separation regions that facilitate more efficient carrier transport and gas-surface interactions. These effects improve key sensing parameters, including sensitivity, selectivity, and response/recovery time. Before exploring the structural categories of HSs, it is important to understand this mechanism as the foundation of their relevance in TMA detection. Several classification schemes of HSs have been proposed in the literature, particularly in comprehensive

reviews such as those by Meng *et al.*[49] and Zappa *et al.*[80] Here, we briefly summarize these categories to provide context for the subsequent analysis, focusing primarily on their implementation in TMA GS. Where possible, we emphasize structural types most commonly reported in the TMA sensing literature.

In general, HSs can be classified into three main types based on their architectural design:

(I) The first type involves a simple blend of two materials that are uniformly distributed throughout the structure, typically indicated by a hyphen between the compounds, such as "ZnO–SnO_2".

(II) The second type features a base material with another material applied or incorporated onto it in some manner, denoted by the "@" symbol. For instance, "ZnO@CuO" indicates that CuO serves as the base material while ZnO is layered or added over it.

(III) The third type of HS is characterized by a distinct boundary or interface between two materials, often denoted by a forward slash. For instance, "ZnO/SnO_2" refers to a bilayer configuration where SnO_2 serves as the bottom layer and ZnO is placed on top. Likewise, "(ZnO–SnO_2)/CuO" describes a composite structure where ZnO and SnO_2 NPs are deposited onto a CuO film, forming a bilayer arrangement.[81,82]

Recently, significant attention has been given to HS NMs because of their influence on various technological fields, with promising results emerging. Hierarchical (branched) nano-HSs have attracted considerable interest because of their superior design, remarkable characteristics, and potential for cutting-edge applications. Traditionally, sensor technologies and industries have been primarily reliant on thin-film technologies. Thin layers of material applied to suitable substrates allow for the replication of material properties on a smaller scale. However, recently, alternatives to these films have been explored. One promising option is the use of one-dimensional (1D) NF/core–shell/polymer composite nano-HSs. Fig. 2 illustrates various categories of HSs. These HSs are critical elements in the advancement of various cutting-edge SC technologies and are vital for optimizing the performance of high-efficiency sensors and detection systems. The primary role of an HS is

to facilitate accurate modulation of the behavior and transport of charge carriers in SCs.[83,84] A basic HS, also called a single HJ, is created by merging SC materials with different chemical compositions according to their positions. The advancement of SC oxide materials with controllable, functional hierarchical HSs has gained significant attention due to their potential to integrate diverse properties based on the morphology, composition, and arrangement of fundamental nanoscale components. More specifically, novel hierarchical HSs incorporating core materials and 1D branches made from various substances show great potential for a broad spectrum of sensor-based applications, particularly in optoelectronic and photonic sensing devices. These advanced HSs offer distinct advantages, enabling the integration of both nanoscale phenomena and enhanced robustness. For example, the epitaxial development of Fe_2O_3/SnO_2 branched HSs could boost sensor performance through the synergistic interaction between the materials (Fe_2O_3 and SnO_2) and their unique branched configuration.[85–89]

3.1. Core–shell HSs

Core–shell HSs have gained significant interest due to their enhanced physical properties compared to individual component materials. These materials are biphasic, consisting of a central core structure surrounded by an external shell, which can be composed of different materials. The combination of the core and shell materials gives rise to unique properties. The shell material is typically engineered to improve the core's thermal stability, reactivity, and resistance to oxidation. Core–shell NMs are widely utilized in various applications, including sensors, energy storage systems, biomedical fields, electronics, and catalysis.[90–94]

3.2. Decorated HSs

GSs using MOSs have been constrained by their elevated operational temperatures and reduced selectivity. To improve the HS performance of these sensors, a typical approach is to decorate or functionalize them with NbMs and MOs, leading to the creation of decorated HSs.[95] These decorated HSs offer several advantages, including a high surface area, synergistic catalytic
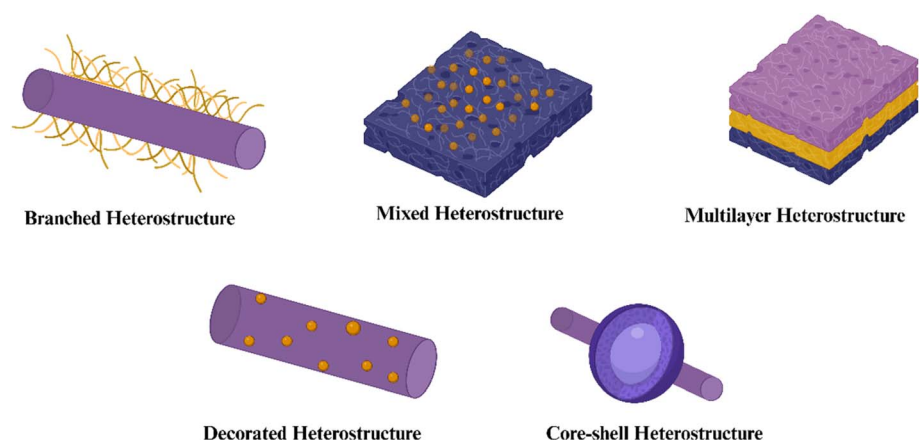

Fig. 2 Schematic diagram of various HS categories.

properties, and the ability to control grain size, all of which improve their sensor functionality. Decorated HSs can influence particle size due to the role of the decorating material in acting as a nucleation center during synthesis. These NPs (*e.g.*, noble metals like Au, Ag, or Pt) can limit the uncontrolled growth of the host material by stabilizing surface energy and interrupting particle agglomeration. As a result, the overall particle size distribution becomes narrower and more controllable. The decorated mesoporous microspheres are typically synthesized through an acid-assisted sol–gel process, where metal alkoxides are dissolved in a solution containing hydrochloric acid, ethanol, and acetic acid. NbM NPs are integrated into the microspheres by dissolving the respective metal salts into the precursor solutions.[96–98] In contrast to traditional post-incorporation techniques, this approach enables the incorporation of metal precursors and the formation of mesostructured materials in a single-step process.[99,100]

To detect fish freshness, Zhang *et al.* developed a SnO$_2$–ZnO nanocomposite GS. By doping SnO$_2$ NPs with 10 wt% ZnO microrods, the GS performance of the sensor was significantly enhanced. The SnO$_2$–ZnO nanocomposite sensor demonstrated high sensitivity to TMA in the 1–500 ppm range at temperatures between 190–330 °C. Additionally, the device demonstrated swift response and recovery kinetics at 330 °C.[20] ZnO microrods provide a high surface area, while SnO$_2$ enhances electronic interactions, making the sensor effective for real-time TMA detection in food safety applications.

In the study performed by Woo *et al.*, ZnO NW GS functionalized with Cr$_2$O$_3$ was utilized for the construction of GS.[72] This sensor synthesized ZnO NWs on alumina substrates and integrated with Au electrodes *via* thermal evaporation. Semi-elliptical Cr$_2$O$_3$ NPs were subsequently deposited onto the surface of the ZnO NWs through the thermal evaporation of CrCl$_2$. The results revealed that the response (R_a/R_g, where R_a represents the resistance in air and R_g denoted the resistance in the target gas) to 5 ppm TMA of the Cr$_2$O$_3$-functionalized ZnO NW sensor was 17.8 at 400 °C. The enhanced sensitivity and selectivity of the sensor toward TMA were attributed to the catalytic effect of the Cr$_2$O$_3$ NPs on the ZnO NW surface and the enlargement of the electron depletion region induced by the p–n junction.[72] Both studies highlighted the importance of HSs in GS performance enhancement. The SnO$_2$–ZnO composite offered a broad detection range, making it suitable for varied TMA concentrations, while the Cr$_2$O$_3$–ZnO NW sensor benefits from p–n junction effects, resulting in high selectivity and sensitivity. However, a key challenge remained: the high operating temperatures (330–400 °C), which limit energy efficiency and practical applications. Future research should explore low temperature operation strategies, such as NbM doping or microfluidic integration, to improve sensor usability in real-world conditions. For this purpose, Zhang *et al.* developed a novel technique for uniformly immobilizing monodispersed Au NPs onto the surfaces of MoO$_3$ nanobelts, which were employed as TMA detection devices. The study examined the influence of Au NP deposition on the TMA-detecting capabilities of MoO$_3$ nanobelts. As a result, the MoO$_3$ nanobelts functionalized with Au NP exhibited markedly enhanced performance,

including improved sensitivity, lower detection threshold, better selectivity, and faster response time, in contrast to pristine MoO$_3$ nanobelts. The engineered sensor demonstrated a peak response of 19.2 to 5 ppm TMA, with a relatively quick response/recovery time of 2/10 seconds and outstanding selectivity at 280 °C.[23] This study highlighted two effective strategies for improving GSs: adjusting material composition and adding catalytic metals. While these approaches improved sensitivity, speed, and selectivity, challenges remain, such as lowering the operating temperature and ensuring long-term durability. Future research could focus on making sensors more energy efficient and integrating AI for real-time calibration, making them more practical for applications like food safety and air quality monitoring.

3.3. Multi-layered HSs

Multi-layered nano-HSs provide a unique approach to enhancing carrier transport properties and achieving a range of customizable characteristics by combining multiple mono-layers. Specifically, graphene nano-HSs offer vast potential for the development of devices in areas such as optoelectronics, sensors, and energy storage. Over the past two decades, 1D HSs have garnered significant interest due to their promising uses in light-driven reactions, detection devices, energy storage, and power conversion. Additionally, particulate hetero-NSs embedded within a polymeric framework present the challenge of ensuring uniform dispersion and consistent bonding of NPs within the framework. Bilayer NMs are considered some of the most essential NSs due to their remarkable electrical, thermal, chemical, mechanical, and optical characteristics. However, a single-layer NM may not demonstrate all of the required features simultaneously.[101,102]

Perillo *et al.* recently developed a bendable GS optimized for operation at reduced temperatures, incorporating TiO$_2$ NT membranes synthesized *via* anodization. These NTs were integrated into a deformable platform, where a network of interwoven Au electrodes was patterned through a standard microfabrication process. The sensor demonstrated the capability to detect TMA within a concentration range of 40–400 ppm, exhibiting a response time of approximately 20–25 seconds.[70] The TiO$_2$ NT structure provided a large surface area for gas adsorption, but the slower response time may limit its suitability for high-speed real-time applications. Nevertheless, the sensor's flexibility and low-temperature operation make it an attractive solution for environments where these characteristics are crucial, such as wearable devices or portable monitoring systems. This study emphasized the importance of novel NSs in improving sensor performance. Interestingly, in a study conducted by Cho *et al.*, a sensor with excellent selectivity and high sensitivity was successfully developed for TMA gas detection using MoO$_3$ nanoplates, which were synthesized *via* ultrasonic spray pyrolysis and subsequently thermally treated at 450 °C. The resulting MoO$_3$ nanoplates, characterized by their small size and gas-permeable structure, exhibited an outstanding sensing performance toward 5 ppm TMA, achieving a resistance ratio (air to gas) of 373.74 at an optimized

operating temperature of 300 °C. Furthermore, the device demonstrated an ultra-low detection limit of 45 ppb.[35] The small size and gas-permeability of the MoO_3 nanoplates significantly enhanced their surface area and adsorption capacity, which likely accounted for the sensor's high sensitivity and rapid detection capability. This approach demonstrated the potential of ultrasonic spray pyrolysis as a scalable, efficient method for creating sensors with low detection limits that are suitable for precise applications like air quality monitoring and food safety. This study emphasized the potential of NbMs and novel NSs in the advancement of high-efficiency sensor TMA. MoO_3 nanoplates provided exceptional sensitivity with a low detection limit, ideal for applications demanding precision. Future research should aim at further optimizing these structures for real world, low-concentration detection, while addressing challenges related to stability and cost-effectiveness for commercial scale application.

3.4. Branched HSs

Branched HSs consist of secondary 1D NWs extending from primary 1D host NWs, creating a branch-like or brush-like configuration. These distinctive structures are particularly fascinating because they share characteristics with decorated HSs that have a very high aspect ratio. While the fabrication of such HSs usually requires several steps, it is often feasible to obtain well-ordered secondary NWs, with some instances showing coherent growth on the host NWs.[103,104]

HS NMs, as a unique variation of 1D NSs, exhibit strong interactions at their closely packed interfaces, leading to improved and more intricate performance. The development of branched HSs that combine p-type and n-type SC MOs offers a crucial approach to integrating the unique characteristics of each separate component into a cohesive structure.[105,106]

In order to detect TMA gas, Yang et al. used Hierarchical structures of Fe_2O_3-like snowflakes in the construction of the sensor. The α-Fe_2O_3 was synthesized using an uncomplicated solvothermal approach, followed by a heat treatment process, exhibiting an outstandingly swift detection and restoration duration (0.9 s/1.5 s) for 100 ppm TMA gas.[69] This rapid performance indicated that the hierarchical structure of Fe_2O_3 significantly improved gas molecule adsorption and surface reaction kinetics, allowing for faster detection. The distinctive snowflake-like structure likely expanded the active interface, optimized engagement with gaseous species, and resulted in a heightened detection performance. This development was notable for its high-speed detection, making it suitable for real-time monitoring of TMA in applications such as food quality control and environmental safety. The hierarchical structure based on Fe_2O_3 exhibited significant advantages in terms of speed and sensitivity. Indeed, this research highlighted the significance of innovative NSs in enhancing sensor efficiency. The study also underscores the potential of hierarchical Fe_2O_3 structures in next-generation GSs, particularly for applications demanding rapid and sensitive detection. Additionally, the unique morphology contributes to improved stability and reproducibility, making it a promising candidate for

commercial sensor development. For example, in a study conducted by Lou et al., a new hierarchical HS of α-Fe_2O_3 NRs and TiO_2 NFs with branch-like NSs was developed to detect TMA gas. This was accomplished through an efficient two-step method involving electrospinning and a hydrothermal process. Furthermore, the investigation assessed the influence of α-Fe_2O_3 loading on TiO_2 NFs and its effect on the TMA sensing performance. The findings indicated that the sensor based on the α-Fe_2O_3/TiO_2 branch-like HSs exhibited a sensitivity ranging from 13.9 to 50 ppm of TMA gas, along with a rapid response and recovery time (0.5 s/1.5 s) at 250 °C.[73] The branch-like structure improved surface area and gas interaction, contributing to its fast-sensing capability. However, while this method enhances response time, further optimization might be needed to improve sensitivity at lower gas concentrations. Future research could focus on combining these strengths, achieving both high sensitivity and rapid response while lowering the operating temperature to enhance energy efficiency. In a recent study by Meng et al., NiO-modified In_2O_3 flower-like (F-L) NSs were successfully fabricated using a straightforward single-step hydrothermal approach and utilized as GSs for TMA detection. The sensor made from 0.05-NiO–In_2O_3 composites with well-defined F-L morphology demonstrated a peak response of approximately 20.5 to 10 ppm TMA at 200 °C, which is 4.7 times greater than that of the pure In_2O_3 F-L NSs, which exhibited a response of 4.4 to 10 ppm TMA.[76] This improvement can be ascribed to the synergistic interaction between NiO and In_2O_3, where NiO enhanced the adsorption of TMA molecules and optimized charge carrier modulation at the p–n HJ. The well-defined F-L morphology further contributed to superior gas diffusion and reaction kinetics, leading to higher sensitivity and efficiency. This study highlighted the potential of HS engineering in optimizing GS performance, particularly in achieving lower operating temperatures and enhanced selectivity. While the branched and flower-like morphologies clearly enhance gas diffusion and surface interaction, the HJs present in these systems also play a critical role in performance improvement. In particular, α-Fe_2O_3/TiO_2 and NiO/In_2O_3 combinations form p–n HJs that facilitate efficient charge separation and band bending at the interface, increasing the sensor's electrical response to electron-donating gases such as TMA. These effects complement the structural advantages and highlight the synergistic impact of both morphology and interfacial electronic properties on sensor performance.

3.5. Hollow HSs

Hollow HSs represent a distinct type of core–shell NS. The term "hollow" refers to structures that feature internal voids or empty spaces, often indicating a considerable amount of free space inside. While any structure with an empty interior can be considered hollow, the term is typically used to describe those with significant vacant space.[105,107,108]

Hollow NSs can be classified into various types based on their shapes and the number of external layers. These include hollow spheres, fibers, tubes, boxes, and other configurations, which differ in overall geometry. Depending on the quantity of

external layers, these structures can be classified as single, double, or multi-shelled (or walled) hollow structures.[109]

Hollow HSs are recognized for their exceptional intrinsic properties, such as magnetic and catalytic behaviors, which make them highly suitable for applications in biosensing, wastewater purification, and ecological restoration. Compared to bulk MO materials, hollow MO-based HSs exhibit superior performance due to their large surface-to-volume ratio, which enhances gas movement and molecular flow within the functional surfaces. Recently, a variety of hollow MO frameworks have been developed for detecting harmful gases, including carbon monoxide, ethanol, hydrogen, liquefied petroleum gas, acetone, and other chemical species.[110,111] In 2012, Kim *et al.* conducted an extensive study on GSs, leading to the development of a TMA GS utilizing Ru–SnO$_2$ hollow spheres. With a shell thickness of around 17 nm, these spheres were synthesized by uniformly depositing Ru- and Sn-precursors onto SiO$_2$ microspheres, each approximately 300 nm in diameter. The Ru–SnO$_2$ hollow spheres showed strong responses to 5 ppm TMA at 350 °C while exhibiting minimal interference from other gases such as toluene, benzene, H$_2$, NH$_3$, C$_3$H$_8$, and CO. The highly sensitive and selective detection of TMA by these Ru–SnO$_2$ hollow spheres was ascribed to GS occurring across the full surface of the shells, coupled with the enhanced catalytic properties imparted by Ru.[112] This study highlighted the importance of material doping and structural design in achieving highly sensitive and selective TMA sensors. Also, hollow spheres provided a large active surface area for gas interaction. Future research could integrate these approaches and combine hollow structures with optimized doping to increase both response time and selectivity at lower operating temperatures.

In addition to the advantages provided by the hollow morphology—such as enhanced surface area and gas diffusion—the interface between Ru and SnO$_2$ in these hollow spheres also plays a key role in boosting sensor performance. This HJ facilitates charge transfer across the interface and enhances the catalytic oxidation of TMA, thereby increasing both sensitivity and selectivity. The synergistic effect between the catalytic activity of Ru and the semiconducting properties of SnO$_2$ highlights the importance of interfacial engineering in hollow HS-based GSs.

3.6. Mixed HSs

Mixed HSs are hybrid materials made by combining two or more different materials at the nanoscale. These materials work together to enhance properties like sensitivity, stability, and efficiency. By combining components such as SCs, metals, or oxides, mixed HSs leverage the strengths of each material, leading to better performance in applications like sensors and energy devices. In these structures, the interface between materials plays a key role, improving charge transfer and enabling faster reactions or better detection. For example, mixing an MO with a noble metal in GSs can improve gas adsorption and response times. These enhanced properties make mixed HSs ideal for applications in fields like environmental monitoring and catalysis. For example, CdO–Fe$_2$O$_3$ NMs were utilized as active sensing components for the GS. The influence of thermal treatment duration and temperature on the GS performance of sensors incorporating CdO–Fe$_2$O$_3$ NMs was further analyzed. The results demonstrated that the sensor responded to 1000 ppm TMA at 230 °C at 1527. This sensor demonstrated a high sensitivity to dilute TMA when operated at 230 °C. Additionally, the response and recovery time for detecting 1000 ppm TMA were 70 seconds and 170 seconds, respectively.[74] This report highlighted the significant impact of thermal treatment on the GS performance of CdO–Fe$_2$O$_3$ sensors, with the results showing high sensitivity to TMA, especially at elevated temperatures. The response time of the sensor and recovery period further emphasize its efficiency in detecting TMA. Future research could focus on optimizing the thermal treatment process to enhance the sensor's response and recovery times while also improving the sensitivity at lower concentrations of TMA. Incorporating advanced NMs or hybrid structures could further boost performance for real time, portable sensing applications. While thermal treatment significantly affects the GS performance of mixed HSs like CdO–Fe$_2$O$_4$, it is important to note that the interface between the two SCs also plays a key role. The p–n junction formed at the interface facilitates charge separation and enhances the reactivity of surface-adsorbed species, especially at elevated temperatures. This synergy between interfacial HJ behavior and thermal effects explains the observed improvements in adsorption and response time. Therefore, the enhanced performance cannot be solely attributed to temperature but rather to the combined effect of structural and thermal factors.

4. HS material

HSs are materials made up of two or more distinct layers or components, each possessing different properties, which are combined to form a single, unified structure. These layers are often composed of different materials, such as SCs, metals, or insulators, and may vary in terms of composition, crystal structure, or thickness. The interaction at the interface between these layers often results in unique physical and chemical properties that are not found in the individual materials.[113–115]

HSs are extensively used across various fields, particularly in electronics, optoelectronics, and materials science. For instance, in SC technology, an HS might involve layers of different various SC materials, like gallium arsenide (GaAs) and aluminum gallium arsenide (AlGaAs), which are utilized in high-performance transistors or lasers. These materials are selected for their differing electronic properties, such as varying band gaps, to achieve specific advantages like enhanced efficiency or better performance.[116,117]

In NMs and nanotechnology, HSs can also refer to hybrid structures that combine different NMs, such as MOS combinations, to improve specific properties like catalytic activity, conductivity, or optical behavior.[118,119] The chosen materials ultimately govern the mechanisms of gas detection, absorption, interactions, and electronic configuration. The characteristics of an ideal material include low cost, high durability, and

extended longevity. The sensor response is typically attributed to the influence of enhanced surface activity (*via* catalysis or adsorption interactions) and charge transfer between HJs with improved performance.[120–122] The size factor is often highlighted as a key factor for enhanced sensitivity and selectivity. A smaller size can elevate sensitivity by restricting charge conduction, similar to how HSs reduce the area in the main conductive pathway of the base material. The HS size should be carefully selected to optimally reduce charge carriers in the main conducting channels. Selectivity can be improved by selecting HS materials that exhibit catalytic capabilities, facilitating surface interactions with gases. This can enhance surface reactivity, as wide-band gap materials are generally less reactive.[96,123–125] The extent of charge depletion in the base material is also affected by the selection of HS materials and their differences in Fermi levels (FLs). Transition MOs and NbMs are often chosen as HS materials to achieve a balance of conduction channel restriction and selective reactivity.[126–128]

4.1. Transition metal oxide

Oxides can function as either n-type or p-type materials (n–pTM), where the majority of charge carriers are either electrons or holes. Most GSs utilize an n-type MO as the core material and combine it with either an n-type or p-type sensing material. However, pTMs are less stable and show a lower response than nTMs due to the formation of a hole-rich region at the surface. In contrast, nTMs exhibit a carrier-depleted region near the surface due to oxygen adsorption. The increased carrier mobility in pTMs mitigates the influence of adsorbed species on resistance. Nonetheless, the incorporation of pTMs with nTMs can enhance sensor performance through increased catalytic activity, additional adsorption sites, the formation of depletion layers, and the creation of electron–hole junctions. These effects can be attributed to two mechanisms: electron transfer limiting conduction and enhanced surface reactivity. When adding pTMs in GSs, it is crucial to consider the reactivity of lattice oxygen, which can engage in surface reactions alongside adsorbed oxygen. This has been demonstrated in catalyst studies using oxygen isotope tracers (O^{18}/O^{16}). The involvement of lattice oxygen in surface reactions is referred to as the Mars–van Krevelen mechanism and is more prevalent in pTMs due to electron loss to bulk oxygen, resulting in reactive surface oxygen. However, this electron loss may also contribute to the gradual decline in the performance of pTMs. Lattice oxygen in SnO_2 has also been found to participate in surface reactions with reducing gases.[129–132]

4.2. Noble metals

NbMs such as Pt, Pd, Au, and Ag have been widely investigated for their ability to improve GS performance owing to their catalytic properties and low FLs. The sensing capabilities are enhanced through functionalization with NbMs *via* electronic and chemical enhancement. Electronic enhancement involves direct interaction between NbMs and MOs, while chemical enhancement focuses on the decomposition of target gas molecules (Fig. 3).[133] When NbMs interact with another
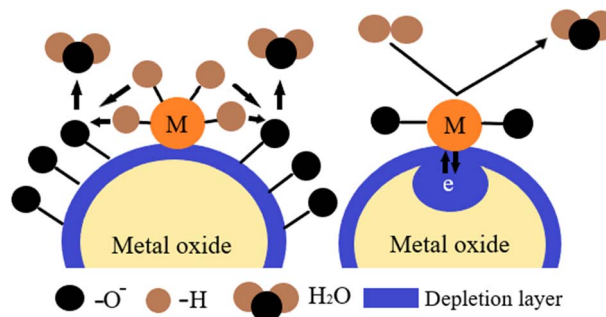

Fig. 3 Electronic and chemical sensitization in functionalization of metal-on-MO.

material, charge transfer takes place until the FLs of both materials are balanced. This leads to electron accumulation in the NbM, generating a depletion zone in the MO. This results in a Schottky barrier with an upward band bending in the MO and a flat band in the NbM. The accumulation of negative charge in the NbM can attract gaseous oxygen. These mechanisms are referred to as enhancement and are commonly used to explain improvements in sensor performance and specificity.[134,135]

5. Synthesis methods of sensor materials

GS materials include MO, SCs, and materials, *etc.* These materials are produced using a variety of processing methods. Some of these methods are outlined below:

5.1. Hydrothermal synthesis

The hydrothermal method, a set of techniques applied to synthesize compounds from elevated-temperature aqueous solutions under increased vapor pressures, involves generating composite materials *via* a heterogeneous chemical process. This reaction occurs in the presence of a solvent at temperatures higher than room temperature and pressures exceeding 1 atmosphere within a sealed system. The result is the formation of materials with high crystallinity and purity. This method can be used to synthesize various materials, such as SCs, catalysts, and NMs, with highly controlled properties due to the precise regulation of temperature, pressure, and solvent conditions. Additionally, it can be utilized to grow single crystals or obtain specific material phases with tailored properties.[136,137] The sensor materials produced through the hydrothermal method are characterized by high purity, with the crystal particle size being easily regulated by fine-tuning reaction conditions such as temperature and pressure. As a result, the fabricated MO NSs exhibit several advantages, such as high purity, uniform crystal particle size, symmetrical crystals, excellent dispersion, tunable structure, adjustable morphology, and environmental compatibility.[138–140] Yao Ji *et al.* recently disclosed high-performance TMA GSs utilizing Co_3O_4/In_2O_3 p–n HSs with novel F-L morphologies created through a one-step hydrothermal approach. The sensor measurements demonstrated

that all sensors exhibited exceptional conductivity for TMA detection at reduced temperatures, with the optimal working temperature for Co_3O_4/In_2O_3 being 200 °C, which is 50 °C lower than that of pure In_2O_3.[141] Zhao *et al.* reported a similar perspective on the role of NbMs in GS fabrication. Considering these key advantages, a highly sensitive TMA GS was engineered by incorporating Au NPs (~4 nm) onto WO_3 nanosheets *via* ultrasonic treatment. The WO_3 nanosheets were prepared through a solvothermal self-assembly approach. The sensor demonstrated an optimal response of 217.72 (R_{air}/R_{gas}) at 300 °C for 25 ppm TMA. Moreover, the Au/WO_3-based sensing platform demonstrated swift response and recovery dynamics (8 s/6 s), an ultrasensitive detection threshold of 0.5 ppm, and outstanding selectivity for TMA detection.[68] The NbM (Au) likely improved the sensor's electronic properties and facilitated electron transport between the sensing interface and gas molecules, contributing to the enhanced response speed and sensitivity. This study highlighted the role of NbMs and innovative NSs in enhancing the development of highly efficient TMA sensors. Also, the Au/WO_3 nanosheet sensor combined selectivity, rapid response, and excellent performance at higher TMA concentrations. These findings underscore the importance of material design and NS engineering in improving sensor performance, with each study contributing valuable insights into enhancing sensitivity, selectivity, and response times in TMA detection.

5.2. Electrospinning

Electrospinning is a highly efficient technique for producing 1D NSs (such as NFs, NWs, NRs, *etc.*) with a highly porous architecture, owing to its benefits of minimal equipment requirements, ease of operation, and remarkable reproducibility.[142–144] This porous configuration provides additional active sites for the adsorption and interaction of TMA vapors within sensing materials. Furthermore, 1D NSs are not constrained to nanoscale dimensions and possess an elevated length-to-diameter ratio, facilitating swift electron transport.[141] MO NSs are fabricated by electrospinning polymer-based solutions containing inorganic precursors, which are then subjected to annealing at temperatures ranging from 400 to 600 °C to eliminate the polymer components.[145–147] In fact, the size and morphology of the resulting NPs can be precisely regulated by manipulating various parameters such as the applied voltage, solution flow rate, and the distance between the spinneret and the collector. This process results in a highly porous structure that enhances TMA molecule diffusion, sensitivity, and response speed. Overall, electrospinning is a versatile and effective method for synthesizing NPs and producing NFs with unique properties for various applications.[148,149] Lee *et al.* fabricated three distinct $ZnO–In_2O_3$ composite NFs with varying compositions using the electrospinning technique to detect TMA gas. All $ZnO–In_2O_3$ composite NFs demonstrated a significant response to TMA. The maximum responses to 5 ppm TMA for the $ZnO–In_2O_3$ composite NFs with compositions of [Zn] : [In] = 67 : 33, 50 : 50, and 33 : 67 at% were 133.9 at 300 °C, 82.9 at 350 °C, and 119.4 at 375 °C, respectively.[58]

5.3. Sol–gel

The sol–gel process stands out as a simple and effective chemical synthesis technique for the creation of high-performance NSd MOs (*e.g.*, SiO_2, TiO_2).[150–152] The process typically involves several key stages, some of which may occur simultaneously. To begin, raw materials are dispersed in solvents such as purified water and/or anhydrous ethanol to trigger the hydrolysis process, generating reactive monomers. Subsequently, the monomers undergo polycondensation to create a colloidal solution, which eventually transforms into a gel with a defined morphological arrangement, experiencing a maturation process. Different dehydration techniques, including super-critical, heat, and freeze-drying, result in varying gel network formations (such as aerogels, xerogels, and cryogels), each influencing the mechanical integrity and sensing characteristics of MO NSs. Aerogels generally exhibit higher surface areas and pore sizes, whereas xerogels demonstrate lower values. Cryogels are characterized by reduced gel contraction. After post-processing treatments like drying and heat treatment, MO NSs are successfully synthesized.[153,154] Finally, the structural characteristics of these NSs are influenced by factors such as solvent type and quantity, concentration of additives, stirring time, aging duration, and calcination conditions, including temperature and time. Among these, the solvent type and quantity play a crucial role in gel formation, while the calcination temperature is vital for controlling pore size and density, which in turn significantly impacts the sensing capabilities of the MO NSs, particularly in detecting TMA vapors.[155–158]

5.4. Chemical vapor deposition (CVD)

Chemical vapor deposition (CVD) is a method used to create a thin film by depositing particles from a gas onto a surface. This process happens in a reaction chamber where gases react at elevated temperatures. A chemical reaction occurs when the heated surface comes into contact with the gas, forming a thin film on the substrate. The result is a highly pure, strong, and uniform material, often used for various high-tech applications. However, CVD comes with challenges, such as needing specialized equipment and handling gases that can be toxic.[159] In research conducted by Nadekar *et al.*, plasma-polymerized thiophene–reduced graphene oxide (PPTh–rGO) composite films were employed to overcome issues related to poor selectivity, prolonged instability, and measurement discrepancies at elevated temperatures. These composite films demonstrated a sensitivity to ammonia and amines that was four times higher than that of the separate PPTh and rGO films. The primary analytes tested for sensing performance included dimethylamine (DMA), ammonia, TMA, and methylamine (MA). At a concentration of 1000 ppm, the sensitivity sequence was found to be MA > ammonia > DMA > TMA. Furthermore, the PPTh–rGO composite films exhibited remarkable selectivity, with a ratio of up to 110 for ammonia and amines when compared to other common VOCs. The response of the sensor remained stable despite temperature fluctuations ranging from 30 °C to 150 °C and sustained consistent performance for more than four months. These results emphasize the promise of

PPTh–rGO composite films in creating highly specific and long-lasting GSs for the detection of ammonia and amines in environmental monitoring.[160]

5.5. Pyrolysis

Pyrolysis is a widely used method for producing NPs, especially in large-scale industrial settings. The process involves heating a chemical compound at high temperatures using a flame and a fast-moving stream of gas or steam.[161] The raw material, either in liquid or vapor form, is pushed into a high-pressure chamber through a small nozzle, where it encounters intense heat. This reaction breaks down the material, and the resulting gases are then separated to collect the NPs. Some systems use lasers or plasma instead of flames to generate the necessary heat. Pyrolysis is popular because it is simple, cost-effective, efficient, and capable of producing high-quality NPs. In a study conducted by Hu *et al.*, graphene quantum dots (GQDs) were synthesized through the thermal decomposition of citric acid, resulting in particle sizes ranging from 2 to 4 nm. The GQDs/α-Fe$_2$O$_3$ composites were fabricated by integrating GQDs with hematite through a simple single-step solvothermal approach. The sensing platform utilizing the GQDs/α-Fe$_2$O$_3$ composite demonstrated a sensitivity of 1033.0 and 1.9 at 270 °C when subjected to TMA vapor concentrations of 1000 ppm and 0.01 ppm, respectively. Remarkably, at 0.01 ppm TMA vapor, the device exhibited an ultra-fast detection time of merely 6 seconds, with a recovery duration of 4 seconds.[162]

5.6. Biosynthesis

Biosynthesis, also known as green synthesis, is an eco-friendly way to produce NPs. This method is safe, biodegradable, and non-toxic, making it a great alternative to traditional chemical processes. Instead of relying on synthetic chemicals, it uses natural sources like plant extracts, bacteria, bacillus, and fungi to create NMs. Because of its sustainable and unique approach, biosynthesis is widely used in biological and medical applications. To monitor the freshness of saltwater fish, Mahata *et al.* developed a GS using a cactus-like NiO NS. They synthesized the sensor material through a simple, low-temperature hydrothermal process. When tested with 10 ppm of TMA, a key indicator of fish spoilage, the sensor demonstrated a 56% response. It reacted within 30 seconds and took 205 seconds to fully recover, making it a promising tool for detecting fish freshness.[163]

5.7. Mechanical milling

Mechanical milling is a widely used method for creating different types of NMs. During production, mechanical grinding helps refine and temper the materials, with various components being milled in a controlled setting. Several factors affect the milling process: plastic deformation, which results in NPs with varying shapes; fractures, which lead to smaller particles; and cold welding, which can cause the NPs to grow larger.[82] Sun *et al.* conducted a significant project using this method. Through a straightforward mechanical grinding approach, montmorillonite underwent surface modification

using tetramethylammonium bromide. Following this alteration, the BET surface area of the treated material (Ball Milling with Tetramethylammonium Bromide for Montmorillonite Modification (BMTMt)) expanded significantly from 20.6 m^2 g^{-1} to 186.4 m^2 g^{-1}, with a microporous fraction reaching 47%. Kinetic uptake experiments demonstrated that BMTMt exhibited superior efficiency in capturing toluene, achieving an adsorption capacity of 55.9 mg g^{-1}-sixfold higher than that of the unmodified counterpart (8.8 mg g^{-1}).[164]

5.8. Nanolithography

Nanolithography is a method used to fabricate exceptionally small structures, generally ranging from 1 nm to 100 nm. Various techniques can be employed to produce NPs, including scanning probe lithography, electron-beam lithography, nano-imprint, optical lithography, and multiphoton lithography. The primary benefit of these techniques is their ability to produce clusters made from a single NM, with precise control over the size and shape of the structures. However, the process typically requires specialized and expensive equipment, and it can be quite complex to operate.[4] For example, top-down Si NT arrays with wall thicknesses ranging from 40 to 10 nm were successfully created using nanoimprint lithography (NIL) and spacer patterning. These NTs, fabricated through the Bosch process, showcased smooth surfaces, extended lengths (∼1000 nm) and remained free from any noticeable distortion or deformation.[165]

5.9. Laser ablation

The hydrothermal approach involves synthesizing materials within a sealed environment where elevated temperatures and pressures facilitate controlled transformations in a solvent medium. This technique enables the formation of structured compounds *via* chemically driven interactions occurring under conditions exceeding ambient temperature and standard atmospheric pressure. This results in materials with high crystallinity and purity material. This method can be employed to create a variety of materials, including SCs, catalysts, and NMs, with highly controlled properties due to the precise manipulation of temperature, pressure, and solvent conditions. The process can also be used to grow single crystals or achieve specific material phases with desired properties.[166]
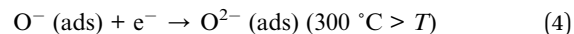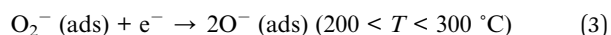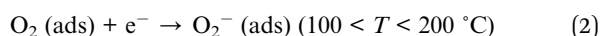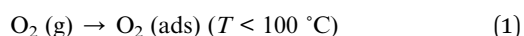
5.10. Sputtering

Sputtering is a method in which NMs are deposited onto a surface by bombarding it with ions, causing material to be ejected from the surface. This technique is commonly used to apply thin films of NMs, which are then often followed by a heating or tempering stage. Factors such as film thickness, temperature range, and reaction time during the process all affect the size and shape of the resulting NMs. Karthikeyan *et al.* utilized a distinct approach to fabricate V$_2$O$_5$ thin layers for DMA gas detection. They examined layers formed under two separate energy inputs, 75 W and 100 W. The layer generated at 100 W exhibited a notable detection behavior in the response curve at ambient conditions across a DMA range of 20 ppm to 100 ppm. The investigation further explored the detection

principle and introduced an applicable methodology for developing NS-integrated resistive chemical sensors.[167] In the research conducted by Park *et al.*, ZnO-based films were fabricated for TMA GS using magnetron sputtering with TiO_2, V_2O_5, or Al_2O_3-doped targets. The film thickness and annealing temperature were identified as crucial parameters for achieving optimal sensitivity and stability. The study demonstrated that doping the films with 1.0 wt% TiO_2, 0.2 wt% V_2O_5, and 4.0 wt% Al_2O_3 enhanced the films' responsiveness and selectivity for TMA gas detection at 300 °C.[75]
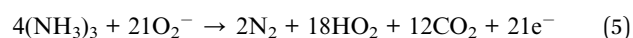
6. Mechanism of MOS GS

The detection process in MO-sensitive materials within GSs relies on the interaction between surface-bound oxygen species and target gas molecules, leading to variations in electrical resistance. In n-type SCs, electrons act as the dominant charge carriers, whereas in p-type counterparts, holes fulfill this role. Upon exposure to atmospheric conditions, oxygen species adhere to the surface of semiconducting MOs, where they capture free electrons and transform into ionic oxygen forms. These negatively charged oxygen species (O^{2-}, O^-, or O^{2-}) undergo ionization through the following reactions:[168]

$$O_2 \text{ (g)} \rightarrow O_2 \text{ (ads)} \ (T < 100 \ ^\circ\text{C}) \tag{1}$$

$$O_2 \text{ (ads)} + e^- \rightarrow O_2^- \text{ (ads)} \ (100 < T < 200 \ ^\circ\text{C}) \tag{2}$$

$$O_2^- \text{ (ads)} + e^- \rightarrow 2O^- \text{ (ads)} \ (200 < T < 300 \ ^\circ\text{C}) \tag{3}$$

$$O^- \text{ (ads)} + e^- \rightarrow O^{2-} \text{ (ads)} \ (300 \ ^\circ\text{C} > T) \tag{4}$$

When a reducing gas interacts with gas molecules and oxygen ions, it causes the formation of a region of electron depletion on the nTM and a region of hole accumulation layer (HAL) on the pTM. The gas molecules and oxygen ions adsorb onto the sensing material's surface and transfer electrons back into the material. This leads to a reduction in the electron depletion layer (EDL), which in turn lowers the resistance in the nTMs.[169] In a similar manner, when it is exposed to oxidizing gases, the opposite process occurs, causing the resistance to increase as the EDL grows. In pTMs, the HAL, which emerges as oxygen molecules capture electrons on the surface, diminishes upon exposure to either reducing or oxidative gases, as illustrated in Fig. 4.

The following equations show the interaction of gas molecules and oxygen ions with a reducing gas (such as TMA):

$$4(NH_3)_3 + 21O_2^- \rightarrow 2N_2 + 18HO_2 + 12CO_2 + 21e^- \tag{5}$$

$$2(NH_3)_3 + 21O^- \rightarrow N_2 + 9HO_2 + 6CO_2 + 21e^- \tag{6}$$

$$2(NH_3)_3 + 21O^2 \rightarrow N_2 + 9HO_2 + 6CO_2 + 42e^- \tag{7}$$

6.1. Factors affecting the sensing mechanism

The resistance of an MO sensor can either increase or decrease when exposed to gaseous species, depending on the specific MO and the type of gas analyte. However, it is crucial to examine the
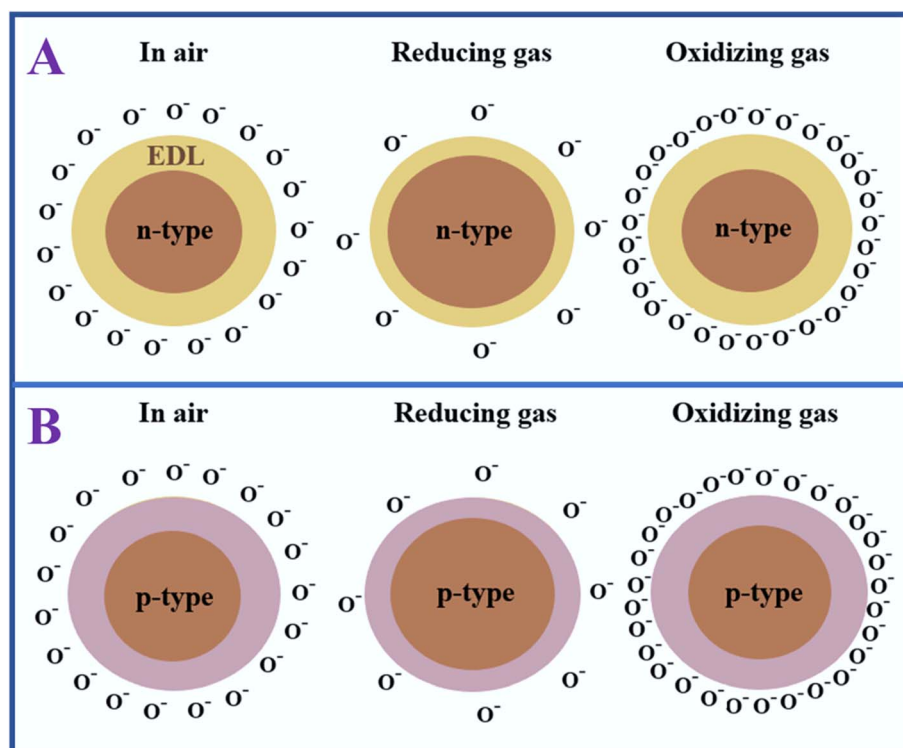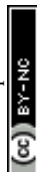

Fig. 4 Variation of the electron depletion region, (A) in n-type and (B) in p-type for reducing gas and oxidizing gas.

underlying junction behavior to understand how different materials impact the performance of the GS.[170–172] As emphasized in the introduction, diverse material compositions can be utilized in developing MO-based GSs. In this regard, interactions between oxide–oxide systems and NbMs with oxides are examined for their gas detection capabilities.[173,174] Key aspects influencing the gas-sensing behavior of these HSs involve the functionality of adsorption-active sites and the interfacial characteristics.[175–178]

6.2. Importance of active adsorption sites

It is reasonable to assume that amplifying the availability of active binding sites on the MO-based detector will enhance its signal output.[80] Furthermore, the nature of the target gaseous species determines which adsorption and release mechanisms are most influential in assessing detection efficiency. In the case of oxidizing gases, superior detection capability is achieved by ensuring extensive molecular interaction at the interface.[179] Given that oxygen possesses strong electronegativity, it withdraws free charge carriers from the detector's interface, thereby reducing conductivity.[180] The presence of oxygen at the interface can be elevated by expanding the exposed area, optimizing binding regions, and limiting molecular detachment.[181] 1D NSs demonstrate a greater surface area relative to their volume when compared to 2D thin films, resulting in enhanced GS performance.[100] Due to their unique morphological features, 1D HSs, such as branched and core–shell configurations, further amplify the active surface area. For instance, α-Fe$_2$O$_3$/TiO$_2$ brush-like NSs fabricated through a solution-based method exhibit a specific surface area of 37 m^2 g^{-1}, which surpasses that of Fe$_2$O$_3$ NWs (7 m^2 g^{-1}), while TiO$_2$ remains void at 21 m^2 g^{-1}. This enables the heterogeneous α-Fe$_2$O$_3$/TiO$_2$ composites to capture a greater number of gas molecules, resulting in a more substantial response compared to TMA. Fig. 5 illustrates FESEM images of α-Fe$_2$O$_3$/TiO$_2$ HSs at various magnifications following a hydrothermal treatment at 95 °C for 4 hours. Occasionally, during the synthesis of HSs, structural imperfections in the

network can increase in parallel with surface area, influencing the sensing behavior.[73]

6.3. Importance of inter-junction between metal oxides

A HJ functions as an electronic and physical interface connecting two distinct solid-state substances. In such HJ, the FLs of the involved materials become aligned, and different or similar charge carriers participate actively in the process. HJs can be categorized into four types depending on the materials involved: MO with MO, MO with metal sulfide, MO with NbMs, and MO with other substances like carbon-based materials (e.g., rGO, g-C$_3$N$_4$, graphene) or rare-earth metals.[181] The formation of an HJ between multiple MOs enhances sensing performance by (a) improving the interaction among electron depletion regions, (b) altering the energy band structure, (c) increasing the number of adsorption sites, and (d) boosting the catalytic activity of the materials.[182] HJs based on MOs can be broadly categorized into two types based on the conduction type of the interfacing materials:

- (Isotype HJs): these occur between SCs of the same type (n–n or p–p). In such junctions, band bending and interfacial charge redistribution influence the transport properties.
- (Anisotype HJs): these form between p-type and n-type SCs (p–n junctions), where a built-in electric field develops due to the diffusion of charge carriers. This leads to the formation of a depletion region, which plays a vital role in enhancing GS performance.

While p–n junctions are widely used in silicon-based electronic devices such as diodes and LEDs, similar principles apply to MO-based sensors, where junctions like NiO–SnO$_2$ or CuO–ZnO improve sensitivity and selectivity via interfacial charge modulation. Integrating diverse materials within an HS opens up new opportunities to enhance the morphological, architectural, and operational characteristics, thereby boosting the performance of the device. When two materials combine to form an HS, their energy levels naturally align as electrons with greater energy move across the interface into available lower-
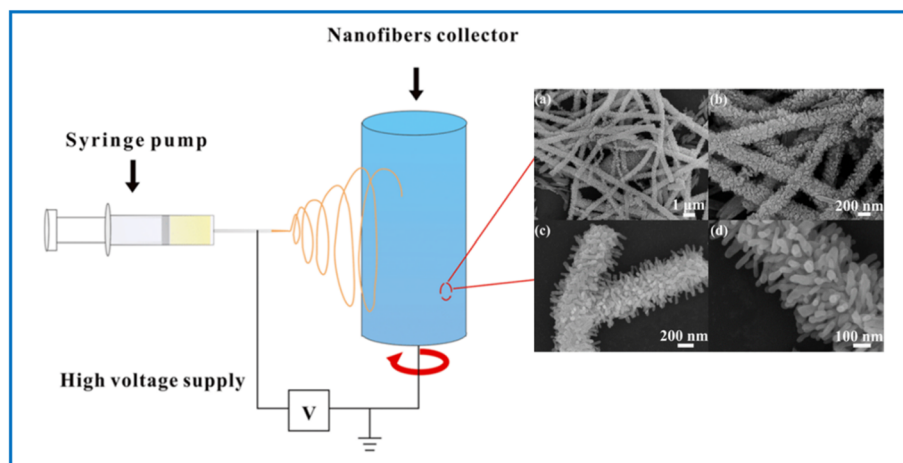

Fig. 5 Schematic diagram of electrospinning process for MO, synthesis FESEM images of the α-Fe$_2$O$_3$/TiO$_2$ HSs: (a and b) panoramic and (c and d) magnified.[73] Permission Copyright © 2013, ACS.

energy states, reaching an equilibrium. This interaction leads to the creation of a depletion zone for charge carriers at the interface. Furthermore, band distortion occurs, establishing an energy barrier due to the initial mismatch between the energy levels of the materials. Consequently, charge carriers need to surmount this energy barrier to pass through the interface, impacting the overall electronic behavior and detection performance of the HS. When a p-type SC forms an HJ with an n-type SC, electrons from the n-type diffuse into the p-type region, while holes from the p-type move into the n-type; this diffusion creates a depletion region near the interface, resulting in the formation of a built-in potential barrier. For p–n junctions, this potential barrier controls the flow of charge carriers, which is crucial in GS applications. In the presence of electron-donating gases such as TMA, the barrier height and the width of the depletion layer are modulated due to surface charge transfer reactions. Adsorption of TMA molecules on the surface can lead to an increase in free electron density (in n-type) or neutralization of holes (in p-type), reducing the barrier and allowing more current to flow. These interfacial changes result in a more pronounced electrical signal, thereby enhancing the sensitivity and selectivity of the GS. A schematic diagram (Fig. 6) has been added to illustrate the energy band diagram and depletion layer behavior before and after gas exposure in a typical p–n HJ.

In an n–n HJ, the interface forms between two semiconducting MOs with different FLs. This creates a flow of electrons from the higher FL (n_1) to the lower FL (n_2), causing band bending until equilibrium is reached.[183] As a result, a potential barrier is formed at the interfaces due to band bending, creating a built-in voltage.[184] When the sensing material is exposed to air, oxygen atoms chemically interact with its surface, resulting in an increase in resistance. On the other hand, in the presence of reducing gases, the adsorbed electrons are released back into the sensing material, causing a decrease in resistance. As a result, gas detection is based on the changes in the resistance of the sensing materials.

In a p–p-type junction, when the FL of one semiconducting MO (P_1) is higher than that of another (P_2), electrons transfer from P_1 to P_2, while holes move from P_2 to P_1. This process results in HAL in P_1 and depletion in P_2, forming a barrier to charge flow. The electric field generated by this movement causes the bands to bend upwards, creating a barrier to charge flow. This barrier varies with the presence of reducing or oxidizing gases, influencing the resistivity. Changes in resistivity correspond to the sensor's sensitivity. Fig. 7 illustrates how electron depletion and accumulation regions in n-HJs, as well as HAL and depletion regions in p–p HJs, vary in response to air and reducing gases.[185]

6.3.1 p–n HJ. As previously discussed, Woo *et al.* developed a GS by synthesizing n-type ZnO NWs coated with p-type Cr_2O_3. Their study demonstrated that the Cr_2O_3 coating effectively narrows the ZnO conduction channel and increases the electrical resistance of the sensor in the air, leading to more pronounced changes upon exposure to TMA, a reducing gas. Moreover, in the continuous core–shell NSs, the primary conduction pathway occurred through the p-type Cr_2O_3 layer. This behavior is attributed to the catalytic role of Cr_2O_3 in facilitating methylamine decomposition, ultimately causing the composite material to exhibit p-type characteristics when interacting with TMA.[72] The GS responses illustrated in Fig. 8(a) and (b) further support this concept. In another notable example, researchers investigated the enhancement of TMA GS performance using NiO-functionalized In_2O_3 F-L structures. The interaction between n-type In_2O_3 and p-type NiO resulted in the formation of p–n HJs at their interface. Since the FL of In_2O_3 is higher than that of NiO, electrons migrate from In_2O_3 to NiO, while holes move in the opposite direction until equilibrium is reached. Consequently, a significantly wider EDL forms at the HJ interface, accompanied by the establishment of a potential barrier. This phenomenon leads to a substantial increase in the resistance of the NiO–In_2O_3 composite, as shown in Fig. 8(c).[47]

6.3.2 n–n and p–p HJ. The establishment of an n–n or p–p HJ results in band bending of energy levels, similar to that observed in p–n junctions. In p–n junctions, resistance increases due to electron–hole recombination at the interface, leading to electron accumulation. Conversely, in an n–n junction, electron transfer occurs from the material with a higher FL to the one with a lower FL. Rather than forming a depletion layer, this process results in the creation of an accumulation layer at the interface (Fig. 9).[186]

The subsequent adsorption of oxygen on the surface depletes the accumulation layer, effectively enhancing the potential energy barrier at the interface and amplifying the sensor's response. Interestingly, an interface between SnO_2 and ZnO was reported by Zhang *et al.*[20] When n-type SnO_2 and n-type ZnO reach equilibrium, electrons migrate from SnO_2 to the lower-energy conduction band of ZnO until their FLs align. This electron transfer induces band bending at the interface. Upon air exposure, oxygen species adsorb onto the surface of the SnO_2–ZnO nano-HSs and ionize into oxygen ions by capturing free electrons. Consequently, a thick depletion layer forms on the oxide surface, increasing the energy barrier at the HJ interface and enhancing TMA sensing performance.
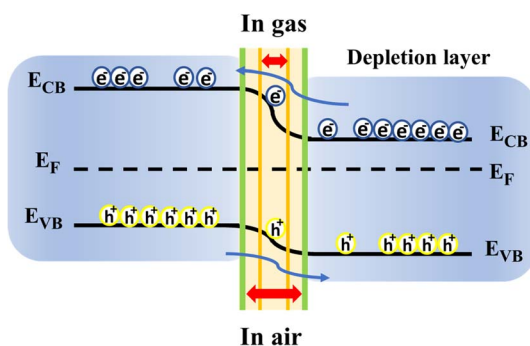
6.4. Importance of doping and HS addition

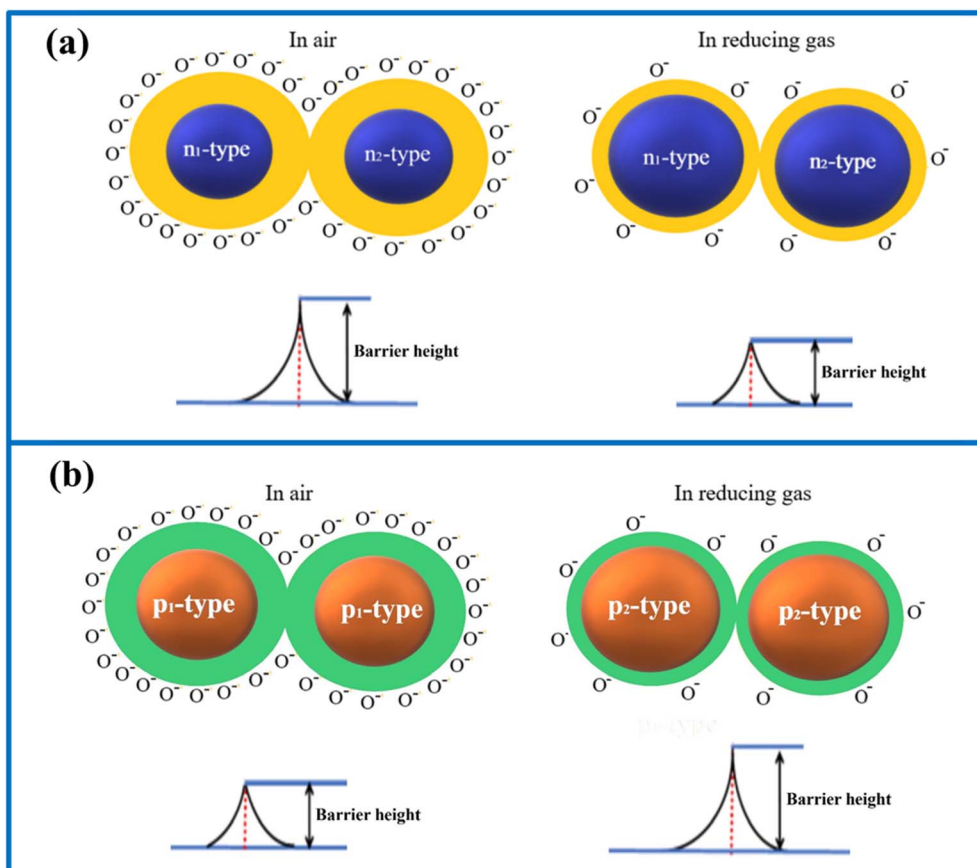Two primary strategies are employed to enhance the performance of GSs: doping and incorporating HSs. The effects of

Fig. 6 The energy band diagram and depletion layer behavior before and after gas exposure in a typical p–n heterojunction.

Fig. 7 Change in barrier height of (a) n–n HJ and (b) p–p HJ in the presence of air and reducing gas.

these methods have been widely investigated under diverse testing conditions and synthesis techniques.[187] The critical factor lies in distinguishing the impacts of doping from those of HJ formation. While HJs promote better separation of charge carriers and widen the depletion region, doping increases the number of active adsorption sites and charge carriers.
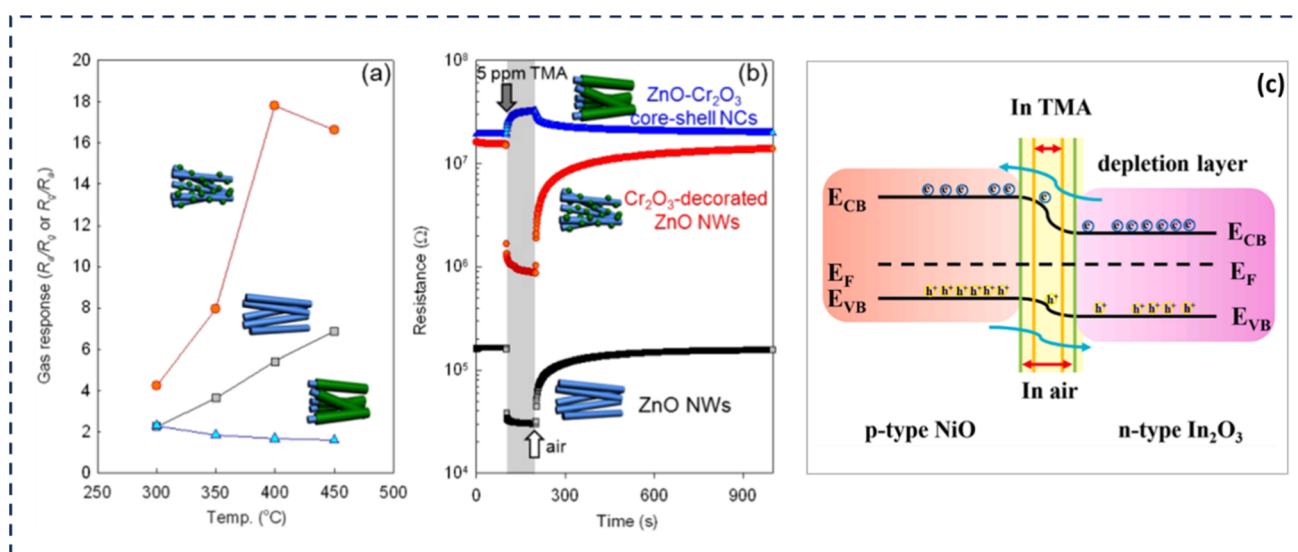
Fig. 8 (a) Gas responses (R_a/R_g or R_g/R_a: R_a, resistance in the air; R_g, resistance in gas) of ZnO NWs, Cr_2O_3-decorated ZnO NWs, and ZnO–Cr_2O_3 core–shell NCs to 5 ppm TMA over the temperature range of 300–450 °C. (b) Dynamic sensing transients to 5 ppm TMA at the sensor temperature of 400 °C.[72] Permission Copyright © 2012, IOP. (c) The proposed energy band structure diagram for NiO–In_2O_3 HJs.[47] Permission Copyright © 2022, Elsevier.

Fig. 9 Energy band diagram of the WO_3–SnO_2 (n–n) HJ at thermal equilibrium.
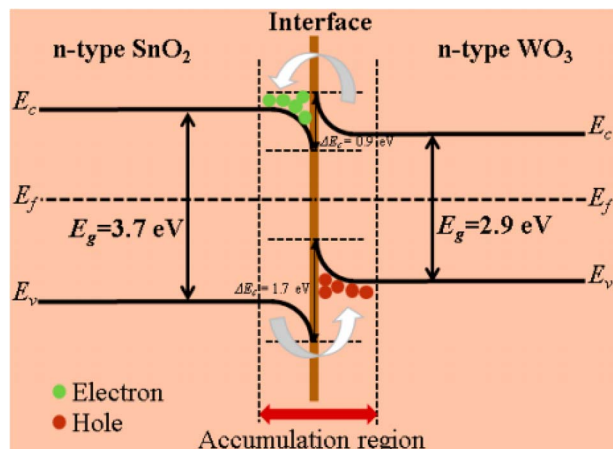
Both methods can be employed to improve selectivity for a particular gas. The introduction of dopant materials into the base material's lattice can notably affect the formation of an HJ. Incorporating a cation into the lattice of various MOs leads to lattice distortion, which can generate adsorption sites for both oxygen and the target gas analyte.[170] Furthermore, the significant improvements in sensing performance, attributed to enhanced chemical and electronic sensitivity, have motivated researchers to investigate the impact of incorporating multiple materials through doping or HS formation. As highlighted in a previous study, n-type In_2O_3 F-L structures were modified with p-type NiO nanograins. The findings revealed that the Ni-decorated sensor exhibited superior performance compared to pure In_2O_3. Additionally, the catalytic activity of NiO was found to accelerate surface reactions, enhancing the real-time gas monitoring process at 200 °C. As illustrated in Fig. 10, the sensor response increases rapidly with rising TMA gas

Fig. 10 The sensor exhibited responses to TMA concentrations ranging from 0.5 to 200 ppm TMA at 200 °C.[47] Permission Copyright © 2022, Elsevier.

concentrations (from 1 to 20 ppm), followed by a gradual decline in the upward trend at higher concentrations. This behavior is likely due to the saturation of TMA adsorption sites at elevated concentrations.

As a result, the 0.05-NiO–In_2O_3 sensor consistently exhibited a higher response than the pure In_2O_3 sensor across all TMA concentrations and was capable of detecting TMA at levels as low as 0.5 ppm (the response was about 1.5), further indicating the sensitization impact of p-type NiO on n-type In_2O_3.[76]

In the case of TMA, a reducing gas with strong electron-donating ability, the described mechanisms are particularly effective. Sensors such as Cr_2O_3-decorated ZnO nanowires[72] and NiO–In_2O_3 composites[76] exhibit pronounced sensitivity to TMA due to synergistic effects at their HJ interfaces. These systems demonstrate enhanced charge transfer, larger depletion widths, and catalytic facilitation of TMA decomposition, making them highly suitable for selective and low-temperature detection of this volatile compound.

7. Microfluidic GSs

Microfluidic GSs are recognized as a modern and efficient approach for achieving high sensitivity, rapid response times, and compact designs. In this type of sensor, microfluidics is integrated with GS technology to significantly enhance the mentioned parameters. In the field of sensors, microfluidic technology allows for the analysis of very small sample volumes, meaning only a tiny amount of reagents or sensing materials is needed.[188] This capability not only makes the process more efficient but also leads to sensors that offer quick responses while requiring minimal sample amounts.[189] There are several reports of integrating MOS sensors with the microfluidic device to realize a miniaturized GS. Martini *et al.* created a microfluidic GS that incorporates a built-in pumping system for detecting ammonia.[190] At the end of the microfluidic channel, there is a tungsten trioxide sensing layer equipped with interdigitated platinum electrodes and a built-in heater. The heater has two key roles: first, it helps maintain a stable temperature for the MO sensing layer, and second, it creates a temperature gradient along the microchannel. The temperature gradient plays a crucial role in driving gas flow through the microfluidic channel, a phenomenon known as thermal creep. For accurate and consistent results, the MOS sensing layer needs to be kept at a stable temperature, which is maintained at an optimal 473 K using a heater. The sensor can detect gas concentrations within a linear range of 10 to 100 ppm. It responds in about 10 minutes, ensuring reliable performance with good reversibility, reproducibility, and baseline stability. 1D sensing NMs, including NWs, NRs, and NTs, offer a large surface area relative to their volume, making them highly sensitive and capable of quickly reacting to analyte molecules. Over the years, there has been a growing body of research focused on the use of these materials for gas-sensing applications. Importantly, 1D-NSs prepared by microfluidics technology have several advantages over traditional bulk methods. It allows for precise control over how the NSs form, reduces the amount of material needed and benefits from smooth, predictable fluid flow. Beyond just
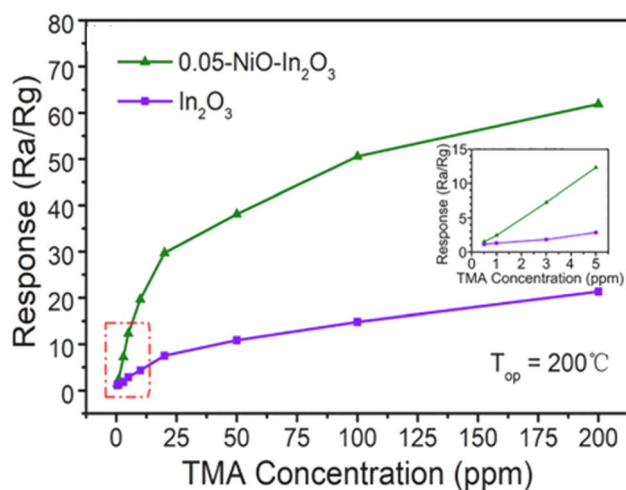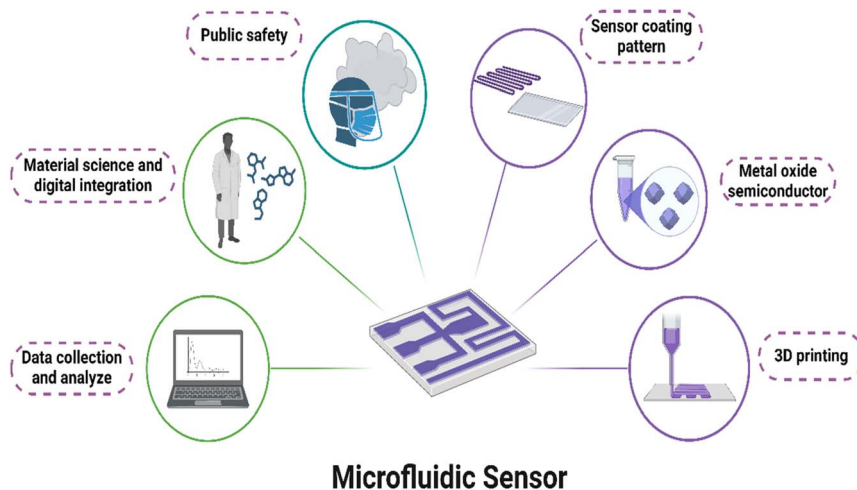
Fig. 11 Schematic of microfluidic GSs: advancing precision detection through cutting edge technology.

making these materials, integrating them into microfluidic chips opens the door to developing a variety of functional microdevices.[191] For example, highly ordered and porous TiO_2 NTs have been manufactured to detect various VOCs. These NTs feature inner diameters ranging from 110 to 150 nm and lengths between 2.5 and 2.7 μm. Their large surface area enhances interactions with analyte molecules, leading to remarkably high sensitivity, with sensor responses reaching approximately 95% within the 0 to 300 ppm concentration range.[192] Microfluidic GSs, despite their numerous advantages, still face several scientific and research challenges. One of the key issues is improving their sensitivity and selectivity to accurately detect specific gases in the presence of other compounds. Additionally, enhancing their stability and longevity under different environmental conditions remains a crucial area of study. Integrating these sensors with electronic and wireless systems can significantly expand their capabilities, but further advancements are needed. Precise control over the synthesis of NMs, such as NWs and NTs, is essential to achieving optimal performance.[59,193,194] Moreover, optimizing the design of microfluidic channels to improve fluid flow and sensing efficiency presents another research challenge. Reducing production costs is also critical for accelerating the commercialization of this technology. Finally, the development of multifunctional sensors capable of detecting multiple gases simultaneously could greatly broaden their range of applications. Advancing this field requires interdisciplinary research across nanotechnology, materials science, chemistry, and electronics.[195,196] Fig. 11 shows the importance of microfluidic GSs in advanced precision detection through advanced technology.

8. The role of artificial intelligence in GSs

The traditional trial-and-error approach to developing high-performance chemiresistive GSs is time-consuming and often inadequate to meet the growing demand for sensors across various industries. Machine learning (ML) can overcome these limitations, offering a more efficient way to improve, develop, and design sensors. Early detection of gas leaks with greater accuracy and reliability using advanced techniques is a crucial technology solution.[197–199] Additionally, identifying specific gases or detecting gases in complex mixtures remains a challenge that requires focused technological innovation. For example, Bilgera et al. proposed combining multiple AI models for gas source localization to identify the leakage point on the ground using six different GSs.[200] Pan et al. introduced a deep learning approach featuring a hybrid framework that combines Convolutional Neural Networks (CNN) and Long Short-Term Memory (LSTM) networks to extract sequential data from transient response curves.[201] Also, Liu et al. discussed two network architectures, Deep Belief Networks, and Stacked Autoencoders, that extract abstract gas features from an electronic nose (E-nose). These features are then used to build Softmax classifiers. The methods they proposed rely on sequential techniques that directly use data from the GSs.[202] Another approach for gas detection involves thermal imaging. When a gas leaks, it causes a rise in temperature compared to normal conditions. This temperature increase can be detected and analyzed using thermal imaging cameras, making it a useful method for identifying leaks.[203] Reserchers proposed a system for detecting methane and ethane gas leaks using a thermal camera.[204] Interestingly, Jadin and Ghazali developed a method for detecting gas leaks using infrared image analysis. Their system uses a series of image processing steps, such as capturing data, preprocessing the images, processing the images, extracting features, and finally classifying the results.[205] The future of artificial intelligence (AI) in GSs looks promising, with advancements that will make them more accurate, efficient, and versatile. AI will help sensors detect specific gases in complex mixtures more precisely, reducing false readings. With real time data processing, these sensors will be able to respond instantly to changes in gas concentrations, improving safety and decision-making. As sensors get smaller and more integrated into smart devices and IoT networks, they will be used in a wider range of industries and applications. AI will also improve the
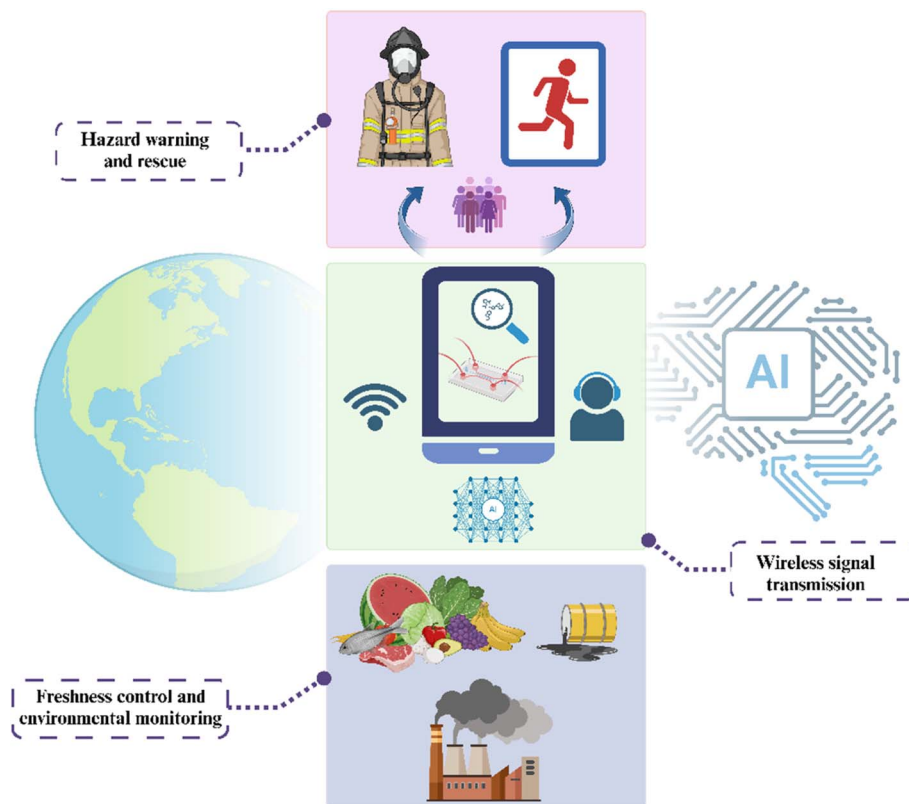
Fig. 12 AI-based GSs: improving the monitoring of global challenges through advanced technologies.

reliability of GSs by predicting when they need maintenance, and multi-sensor networks will offer more detailed and comprehensive monitoring.[206,207] Additionally, AI will optimize energy efficiency, extending the battery life of sensors and allowing them to function in remote or hard-to-reach areas. In the end, AI will make GSs smarter and more adaptable, helping to improve safety, environmental monitoring, and industrial processes (Fig. 12).[208,209]

Although the use of AI in gas sensing is steadily advancing, recent approaches have started moving beyond general concepts. Researchers are now exploring more targeted applications like improving selectivity, optimizing sensor design, and enabling smarter deployment in real-world conditions.[210]

8.1. AI-driven selectivity modeling for TMA detection

Recent studies have shown that machine learning models—such as support vector machines and ensemble classifiers—can be effectively trained to distinguish TMA from structurally similar amines based on subtle differences in dynamic sensor response patterns. This selectivity optimization is particularly valuable for food freshness monitoring, where the presence of multiple nitrogen-based volatile compounds can interfere with accurate detection.

8.2. Digital twin technology for GSs

The integration of digital twin technology in gas sensing systems is an emerging trend. By simulating the real-time behavior and aging process of sensors through AI-based models, these virtual replicas allow for adaptive calibration and predictive maintenance especially beneficial for continuous monitoring of perishable goods emitting TMA.

8.3. AI-enhanced fabrication process optimization

AI tools, including Bayesian optimization and reinforcement learning, are increasingly being used to fine-tune fabrication parameters such as dopant ratios, synthesis temperature, and reaction time. This data-driven control strategy enables researchers to customize the morphology and surface chemistry of MOH-based sensors for enhanced responsiveness to TMA.

8.4. TMA-specific datasets and open-source training platforms

The development of open-access datasets specifically curated for TMA sensing—under varying conditions of concentration, temperature, and humidity—has opened new possibilities for collaborative model training. Such initiatives provide standardized benchmarks for evaluating AI algorithms across diverse sensor platforms.

8.5. Federated learning for distributed IoT sensor networks

In practical deployments such as smart packaging or indoor air quality monitoring in seafood markets, federated learning allows edge sensors to learn from local data while contributing

Table 2 Structural and performance attributes of TMA GSs based on HS materials

Morphology	Material system	Synthesis method	TMA (ppm)	Temperature (°C)	Response/ recovery (s)	Key advance	Ref.
Decorated	$Au@WO_3$	Hydrothermal	100	280	7/6	High response fast kinetics	54
Core–shell	$Cr_2O_3@ZnO$ NWs	Thermal evaporation	5	400	—	High selectivity via p–n interface	60
Nanocomposite	SnO_2–ZnO	Hydrothermal	1–500	330	—	Wide detection range	20
Branched	α-Fe_2O_3/TiO_2	Electrospinning + hydrothermal	50	250	0.5/1.5	Ultra-fast response	61
Mixed	CdO–Fe_2O_3	Co-precipitation	1000	230	70/170	High sensitivity at high concentration	62
Core–shell	NiO–In_2O_3	Hydrothermal	10	200	—	Lower temp; enhanced adsorption	64
Hollow	Ru–SnO_2	Template + chemical deposition	5	350	—	Highly selective; large surface area	97
Multilayered	TiO_2 NTs	Electrochemical anodization	40–400	80	$\sim$20–25	Flexible, low-temp sensor	58
Ultrafine nanoplate	MoO_3	Ultrasonic spray pyrolysis	5	300	—	Ultra-low detection limit (45 ppb)	34
Decorated	$Au@MoO_3$	Hydrothermal	5	280	2/10	Improved selectivity and fast response	23

to a global model—without transferring raw data to central servers. This approach enhances privacy and enables context-aware TMA detection in decentralized networks.

9. Comparative analysis of MOH structures in TMA sensing

In order to better highlight the relevance of existing studies to TMA detection, Table 2 summarizes key sensor configurations, their structural types, synthetic methods, and performance characteristics such as response time, detection limit, and optimal operating temperature. The performance of HSs appears to be highly dependent on morphology, with branched and core–shell structures generally providing faster response/recovery due to enhanced gas diffusion and surface area, while decorated and doped systems show improved selectivity due to catalytic enhancement. Notably, NiO–In_2O_3 and Cr_2O_3–ZnO p–n HSs exhibited superior TMA sensitivity at relatively low temperatures, suggesting that energy-efficient designs can be realized through interface engineering. These comparisons support the argument that HS classification is not merely a structural taxonomy but a basis for predicting and optimizing TMA sensing behavior.

10. Conclusion and future trends

In this review, we summarized the progress made in the development of based GSs with a specific focus on the detection of TMA, a key indicator of food spoilage. Various types of HSs—including core–shell, decorated, branched, hollow, and multilayer configurations—have demonstrated enhanced GS properties through synergistic effects in charge transport, surface activity, and interfacial modulation. While significant advancements have been made in terms of sensitivity and detection limits, current MOH-based sensors still face

challenges such as selectivity in mixed-gas environments, high operating temperatures, long-term drift, and issues with reproducibility across batches. Moreover, the lack of standard protocols and real-world validation limits their commercial readiness. Also, in this review article, the importance of microfluidic sensors was discussed in order to improve the main parameters and their development in the sensing of TMA. Because the use of this type of sensor improves factors such as sensitivity, selectivity, and response time, these sensors will indeed become key in monitoring air, water, and soil quality in real time. These sensors, integrated with AI and IoT, will provide continuous environmental data, enabling rapid response to pollution or hazardous conditions.[211–213] With their ability to detect gases at extremely low concentrations, they can be used to monitor air pollutants, such as CO_2, methane, or VOCs, on a global scale. Ultimately, understanding the relationships between surface reactions, HJ interfaces, morphology, and the sensor environment is crucial for advancing sensor technology and other technologies utilizing MOSs. AI is particularly valuable in areas where precision is essential, such as detecting hazardous gases in industrial settings or monitoring air quality.[214] Also, it enables real time data analysis, which means sensors can quickly alert users to dangerous conditions, improving safety and response times. AI also contributes to the longevity of GSs by predicting when maintenance is needed, reducing downtime, and preventing costly repairs.[215] Essentially, the combination of AI and GS technology is revolutionizing how we monitor and respond to the world around us.[216]

This review also highlights various challenges and provides insight into how to address these issues. MO sensors are highly sensitive and can detect a wide range of chemical compounds, but their main drawback is poor selectivity. They often respond to multiple gases at once, which can lead to inaccurate readings or false alarms, especially in environments with mixed

pollutants. Their performance is also influenced by factors like shape, crystal structure, and surface area, making selectivity a critical challenge. A promising way to tackle this issue is by developing MOHs. By combining different MOs, researchers can create materials that are more finely tuned to detect specific gases while filtering out unwanted interference. These HSs can be designed to enhance surface reactions and improve their interaction with target molecules. Another effective approach is doping these materials with transition or NbMs, which helps refine their selectivity by tweaking their electronic properties and making them more receptive to particular gases. Many MO sensors struggle with slow response times, meaning they take longer to detect changes in gas levels. This can be a major drawback in situations where rapid detection is crucial. On top of that, their stability tends to decline over time, especially in harsh conditions like high humidity or extreme temperatures. These factors can make long-term monitoring unreliable.

A smart way to overcome these challenges is by integrating gas microfluidic sensors with AI and IoT technology. These advanced sensors can be engineered to detect and analyze gases more efficiently by optimizing material properties, such as increasing surface area to enhance gas interactions. Microfluidic sensors also improve gas transport, helping them respond more quickly. By incorporating ML and AI, these systems can adjust for environmental factors like temperature changes, ensuring more stable and reliable performance over time. Many modern sensors consume a lot of power, which can make them impractical for remote or off-grid locations. High energy demands also create challenges for integrating them into compact, portable devices, especially for environmental monitoring where low-power operation is essential. A practical solution is to develop energy-efficient sensor systems. By using advanced materials like thin films or nanoscale structures, sensors can function effectively while consuming less power. Another promising approach is integrating energy harvesting technologies, such as solar power, to support long-term, autonomous operation. These innovations make sensors more adaptable for continuous monitoring without relying heavily on external power sources. Traditional chemical sensors often struggle with real-time data processing, meaning the information they collect isn't always immediately useful. This can be a serious issue in situations where quick action is needed, such as detecting gas leaks or sudden pollution spikes. A smart solution is to integrate AI and IoT into these sensor systems. With AI, sensors can analyze data patterns, quickly spot anomalies, and send instant alerts when something goes wrong. IoT connectivity takes it a step further by enabling remote monitoring, so users can track environmental conditions and respond in real time from anywhere. This combination not only improves speed and accuracy but also makes sensors far more efficient and reliable in critical situations. GSs often face challenges in real world environments, like industrial sites or outdoor air monitoring, where factors such as temperature shifts, humidity, and other environmental changes can affect their accuracy. These fluctuations can lead to unreliable readings, making it harder to trust the data they provide. A smart way to enhance sensor resilience is by using protective

coatings or encapsulation techniques to shield them from harsh conditions. Additionally, AI-driven calibration can help sensors adapt to environmental changes in real time. With ML algorithms, sensors can automatically adjust their readings, ensuring they stay accurate and reliable no matter the conditions. MO sensors often face durability issues, as their performance can decline over time due to constant exposure to gases and environmental conditions. This wear and tear can lead to sensor failures or reduced accuracy, which is a major problem for applications that rely on continuous, long-term monitoring. To address this, researchers are working on stronger and more resilient sensor materials. One approach is designing HSs with reinforced physical structures or adding protective layers to slow down degradation. Additionally, AI and IoT technologies can help monitor sensor health, predicting when maintenance or replacements are needed. This proactive approach helps prevent unexpected failures, ensuring the sensors remain reliable over time.

Abbreviations

TMA	Trimethylamine
GS	Gas sensor
HPLC	High-performance liquid chromatography
MOS	Metal oxide semiconductor
MOH	Metal oxide heterostructure
GC-MS	Gas chromatography-mass spectrometry
IMS	Ion mobility spectrometry
AlGaAs	Aluminum gallium arsenide
GaAs	Gallium arsenide
PPTh	Plasma-polymerized thiophene
rGO	Reduced graphene oxide
MA	Methylamine
DMA	Dimethylamine
GQDs	Graphene quantum dots
BMTMt	Ball milling with tetramethylammonium bromide for montmorillonite modification
NIL	Nanoimprint lithography
EDL	Electron depletion layer
HAL	Hole accumulation layer
Al	Artificial intelligence
ML	Machine learning
CNN	Convolutional neural networks
LSTM	Long short-term memory
E-nose	Electronic nose
NM	Nanomaterial
NP	Nanoparticle
NR	Nanorod
NF	Nanofiber
NW	Nanowire
MO	Metal oxide
IOT	Internet of things
VOC	Volatile organic compound
SC	Semiconductor
HS	Heterostructure

Data availability

Access to the data used in this study is available upon request and may be subject to approval by the data provider. Restrictions may apply to the availability of these data, which were used under license for this study. Interested parties are encouraged to contact the corresponding author for further information on accessing the data. Access to some data may be restricted due to privacy or ethical restrictions. Any restrictions to data availability will be disclosed at the time of data request.

Author contributions

K. K.: investigation, writing – original draft, A. F.: investigation, writing – review & editing, H. S. A.: validation, interpretation of data, supervision, writing – review & editing, M. H.: conceptualization, design of the work, interpretation of data, writing – review & editing, all authors read and approved the final manuscript.

Conflicts of interest

The authors declare no competing interests.

Acknowledgements

References

1 E. De Boeck, L. Jacxsens, M. Bollaerts, M. Uyttendaele and P. Vlerick, Interplay between food safety climate, food safety management system and microbiological hygiene in farm butcheries and affiliated butcher shops, *Food Control*, 2016, **65**, 78–91.

2 L. Fonseca and C. Cané, Chapter 13 – Monitoring perishable food, in *Advanced Nanomaterials for Inexpensive Gas Microsensors*, ed. Llobet E., Elsevier, 2020, pp. 289–314.

3 H. Yu, C. Guo, X. Zhang, Y. Xu, X. Cheng, S. Gao, *et al.*, Recent development of hierarchical metal oxides based gas sensors: From gas sensing performance to applications, *Adv. Sustainable Syst.*, 2022, **6**(4), 2100370.

4 R. J. Rath, S. Farajikhah, F. Oveissi, F. Dehghani and S. Naficy, Chemiresistive sensor arrays for gas/volatile organic compounds monitoring: a review, *Adv. Eng. Mater.*, 2023, **25**(3), 2200830.

5 L.-X. Ou, M.-Y. Liu, L.-Y. Zhu, D. W. Zhang and H.-L. Lu, Recent progress on flexible room-temperature gas sensors based on metal oxide semiconductor, *Nano-Micro Lett.*, 2022, **14**(1), 206.

6 S. F. Hamilton, T. J. Richards and B. E. Roe, Chapter 85 – Food Waste: Farms, distrubtors, retailers, and households, in *Handbook of Agricultural Economics*, ed. Barrett C. B. and Just D. R., Elsevier, 2022, vol. 6, pp. 4653–4703.

7 H. N. Onyeaka and O. F. Nwabor, Chapter 2 – Food ecology and microbial food spoilage, in *Food Preservation and Safety of Natural Products*, ed. Onyeaka H. N. and Nwabor O. F., Academic Press, 2022, pp. 3–18.

8 A. Mirzaei, Z. Kordrostami, M. Shahbaz, J.-Y. Kim, H. W. Kim and S. S. Kim, Resistive-based gas sensors using quantum dots: A review, *Sensors*, 2022, **22**(12), 4369.

9 B. Yang, N. V. Myung and T. T. Tran, 1D metal oxide semiconductor materials for chemiresistive gas sensors: a review, *Adv. Electron. Mater.*, 2021, **7**(9), 2100271.

10 J. T. Keeton and M. E. Dikeman, 'Red' and 'white' meats— terms that lead to confusion, *Anim. Front.*, 2017, **7**(4), 29–33.

11 M. McWilliams, Meats, poultry, and fish, *Foods: Experimental Perspectives*, 2012, pp. 253–285.

12 S. Chen, N. Gao, B. R. Bunes and L. Zang, Tunable nanofibril heterojunctions for controlling interfacial charge transfer in chemiresistive gas sensors, *J. Mater. Chem. C*, 2019, **7**(44), 13709–13735.

13 T. Liu, W. Zhang, M. Yuwono, M. Zhang, M. Ueland, S. L. Forbes, *et al.*, A data-driven meat freshness monitoring and evaluation method using rapid centroid estimation and hidden Markov models, *Sens. Actuators, B*, 2020, **311**, 127868.

14 X. Gu, L. Feng, J. Zhu, Y. Li, K. Tu, Q. Dong, *et al.*, Application of gas sensors for modelling the dynamic growth of Pseudomonas in pork stored at different temperatures, *Meat Sci.*, 2021, **171**, 108282.

15 R. Upadhyay, S. Sehwag and H. N. Mishra, Electronic nose guided determination of frying disposal time of sunflower oil using fuzzy logic analysis, *Food Chem.*, 2017, **221**, 379–385.

16 O. O. Alegbeleye, I. Singleton and A. S. Sant'Ana, Sources and contamination routes of microbial pathogens to fresh produce during field cultivation: A review, *Food Microbiol.*, 2018, **73**, 177–208.

17 Y. Kou, L. Hua, W.-J. Chen, X. Xu, L. Song, S. Yu, *et al.*, Material design and application progress of flexible chemiresistive gas sensors, *J. Mater. Chem. A*, 2024, **12**(33), 21583–21604.

18 S. Wang, H. Chen and B. Sun, Recent progress in food flavor analysis using gas chromatography–ion mobility spectrometry (GC–IMS), *Food Chem.*, 2020, **315**, 126158.

19 A. B. Falowo, P. O. Fayemi and V. Muchenje, Natural antioxidants against lipid–protein oxidative deterioration in meat and meat products: A review, *Food Res. Int.*, 2014, **64**, 171–181.

20 W.-H. Zhang and W.-D. Zhang, Fabrication of SnO2–ZnO nanocomposite sensor for selective sensing of trimethylamine and the freshness of fishes, *Sens. Actuators, B*, 2008, **134**(2), 403–408.

21 A. Sharma, S. B. Eadi, H. Noothalapati, M. Otyepka, H.-D. Lee and K. Jayaramulu, Porous materials as effective

chemiresistive gas sensors, *Chem. Soc. Rev.*, 2024, **53**(5), 2530–2577.

22 Y. Chen, X. Li, C. Zhu, G. Fan, S. Khademolqorani and S. N. Banitaba, Recent insights on MXene-based architectures for monitoring and sensing of gaseous pollutants: A review, *Talanta*, 2024, **280**, 126700.

23 J. Zhang, P. Song, Z. Li, S. Zhang, Z. Yang and Q. Wang, Enhanced trimethylamine sensing performance of single-crystal MoO3 nanobelts decorated with Au nanoparticles, *J. Alloys Compd.*, 2016, **685**, 1024–1033.

24 K. Mitsubayashi, Y. Kubotera, K. Yano, Y. Hashimoto, T. Kon, S. Nakakura, *et al.*, Trimethylamine biosensor with flavin-containing monooxygenase type 3 (FMO3) for fish-freshness analysis, *Sens. Actuators, B*, 2004, **103**(1), 463–467.

25 G. M. Bota and P. B. Harrington, Direct detection of trimethylamine in meat food products using ion mobility spectrometry, *Talanta*, 2006, **68**(3), 629–635.

26 H. Cai, X. Qiao, M. Chen, D. Feng, A. A. Alghamdi, F. A. Alharthi, *et al.*, Hydrothermal synthesis of hierarchical SnO2 nanomaterials for high-efficiency detection of pesticide residue, *Chin. Chem. Lett.*, 2021, **32**(4), 1502–1506.

27 C. Cai, J. Mo, Y. Lu, N. Zhang, Z. Wu, S. Wang, *et al.*, Integration of a porous wood-based triboelectric nanogenerator and gas sensor for real-time wireless food-quality assessment, *Nano Energy*, 2021, **83**, 105833.

28 W. Ren, C. Zhao, G. Niu, Y. Zhuang and F. Wang, Gas sensor array with pattern recognition algorithms for highly sensitive and selective discrimination of trimethylamine, *Adv. Intell. Syst.*, 2022, **4**(12), 2200169.

29 M. Wusiman and F. Taghipour, Methods and mechanisms of gas sensor selectivity, *Crit. Rev. Solid State Mater. Sci.*, 2022, **47**(3), 416–435.

30 M. A. Babazad, A. Foroozandeh, M. Abdouss, H. SalarAmoli, R. A. Babazad and M. Hasanzadeh, Recent progress and challenges in biosensing of carcinoembryonic antigen, *TrAC, Trends Anal. Chem.*, 2024, 117964.

31 S. Petričević, N. Marušić Radovčić, K. Lukić, E. Listeš and H. Medić, Differentiation of dry-cured hams from different processing methods by means of volatile compounds, physico-chemical and sensory analysis, *Meat Sci.*, 2018, **137**, 217–227.

32 Z. Chen, Y. Lin, X. Ma, L. Guo, B. Qiu, G. Chen, *et al.*, Multicolor biosensor for fish freshness assessment with the naked eye, *Sens. Actuators, B*, 2017, **252**, 201–208.

33 S. Jiang and Y. Liu, Gas sensors for volatile compounds analysis in muscle foods: A review, *TrAC, Trends Anal. Chem.*, 2020, **126**, 115877.

34 Y. H. Cho, Y. C. Kang and J.-H. Lee, Highly selective and sensitive detection of trimethylamine using WO3 hollow spheres prepared by ultrasonic spray pyrolysis, *Sens. Actuators, B*, 2013, **176**, 971–977.

35 Y. H. Cho, Y. N. Ko, Y. C. Kang, I.-D. Kim and J.-H. Lee, Ultraselective and ultrasensitive detection of trimethylamine using MoO3 nanoplates prepared by

ultrasonic spray pyrolysis, *Sens. Actuators, B*, 2014, **195**, 189–196.

36 X. Chu, Y. Han, S. Zhou and H. Shui, Trimethylamine sensing properties of nano-SnO2 prepared using microwave heating method, *Ceram. Int.*, 2010, **36**(7), 2175–2180.

37 J. Fiori, S. Turroni, M. Candela, P. Brigidi and R. Gotti, Simultaneous HS-SPME GC-MS determination of short chain fatty acids, trimethylamine and trimethylamine N-oxide for gut microbiota metabolic profile, *Talanta*, 2018, **189**, 573–578.

38 Z. Hua, C. Tian, Z. Qiu, Y. Li, X. Tian, M. Wang, *et al.*, An investigation on NO2 sensing mechanism and shielding behavior of WO3 nanosheets, *Sens. Actuators, B*, 2018, **259**, 250–257.

39 K. L. A. Kumar, S. Durgajanani, B. G. Jeyaprakash and J. B. B. Rayappan, Nanostructured ceria thin film for ethanol and trimethylamine sensing, *Sens. Actuators, B*, 2013, **177**, 19–26.

40 J. Shen, S. Xu, C. Zhao, X. Qiao, H. Liu, Y. Zhao, *et al.*, Bimetallic Au@Pt Nanocrystal Sensitization Mesoporous α-Fe2O3 Hollow Nanocubes for Highly Sensitive and Rapid Detection of Fish Freshness at Low Temperature, *ACS Appl. Mater. Interfaces*, 2021, **13**(48), 57597–57608.

41 R. Kumari and R. Kumar, recent advances in MoS2 and its derivatives-based two-dimensional gas sensors, *ECS J. Solid State Sci. Technol.*, 2022, **11**(9), 097003.

42 T. Yang, H. Yu, B. Xiao, Z. Li and M. Zhang, Enhanced 1-butylamine gas sensing characteristics of flower-like V2O5 hierarchical architectures, *J. Alloys Compd.*, 2017, **699**, 921–927.

43 X. Chu, J. Wang, Q. Gao, Y. Wang, S. Liang, L. Bai, *et al.*, High selectivity trimethylamine sensors based on graphene-NiGa2O4 nanocomposites prepared by hydrothermal method, *Phys. E*, 2020, **118**, 113788.

44 P. Wang, Z. Zheng, X. Cheng, L. Sui, S. Gao, X. Zhang, *et al.*, Ionic liquid-assisted synthesis of α-Fe 2 O 3 mesoporous nanorod arrays and their excellent trimethylamine gas-sensing properties for monitoring fish freshness, *J. Mater. Chem. A*, 2017, **5**(37), 19846–19856.

45 K. Dashtian, F. Zahedpour, A. Foroozandeh, R. Karimi, M. Abdouss and S. Hajati, Recent Trends in Molecularly Imprinted Photoelectrochemical Sensors, *TrAC, Trends Anal. Chem.*, 2025, 118271.

46 D. Kishore Kumar, K. Raghava Reddy, V. Sadhu, N. P. Shetti, C. Venkata Reddy, R. S. Chouhan, *et al.*, 4 – Metal oxide-based nanosensors for healthcare and environmental applications, in *Nanomaterials in Diagnostic Tools and Devices*, ed. Kanchi S. and Sharma D., Elsevier, 2020, pp. 113–129.

47 A. Foroozandeh, M. A. Babazad, S. Jouybar, M. Abdouss, H. SalarAmoli, K. Dashtian, *et al.*, Recent advancements in nanobiosensors for diagnosis of ovarian cancer: Analytical approaches, *TrAC, Trends Anal. Chem.*, 2024, 118119.

48 A. Moumen, G. C. W. Kumarage and E. Comini, P-Type Metal Oxide Semiconductor Thin Films: Synthesis and Chemical Sensor Applications, *Sensors*, 2022, **22**(4), 1359.

49 F.-J. Meng, R.-F. Xin and S.-X. Li, Metal oxide heterostructures for improving gas sensing properties: a review, *Materials*, 2022, **16**(1), 263.

50 Y. S. Do, Y. Myung and C. W. Na, Highly Sensitive sub-ppm level Trimethylamine Gas Sensor Based on Porous CuO/In₂O₃ Nanostructures, *J. Sens. Sci. Technol.*, 2024, **33**(5), 305–309.

51 L. Hou, J. Duan, F. Xiong, C. Carraro, T. Shi, R. Maboudian, et al., Low Power Gas Sensors: From Structure to Application, *ACS Sens.*, 2024, **9**(12), 6327–6357.

52 S. Uma and M. K. Shobana, Band structure and mechanism of semiconductor metal oxide heterojunction gas sensor, *Inorg. Chem. Commun.*, 2024, **160**, 111941.

53 P. Zhu, Y. Wang, P. Ma, S. Li, F. Fan, K. Cui, et al., Low-power and high-performance trimethylamine gas sensor based on nn heterojunction microbelts of perylene diimide/CdS, *Anal. Chem.*, 2019, **91**(9), 5591–5598.

54 M. Ma, X. Yang, X. Ying, C. Shi, Z. Jia and B. Jia, Applications of gas sensing in food quality detection: A review, *Foods*, 2023, **12**(21), 3966.

55 A. Singh, S. Sikarwar, A. Verma and B. C. Yadav, The recent development of metal oxide heterostructures based gas sensor, their future opportunities and challenges: a review, *Sens. Actuators, A*, 2021, **332**, 113127.

56 M. Egashira, Y. Shimizu and Y. Takao, Trimethylamine sensor based on semiconductive metal oxides for detection of fish freshness, *Sens. Actuators, B*, 1990, **1**(1), 108–112.

57 L. Liu, P. Song, Z. Yang and Q. Wang, Highly sensitive and selective trimethylamine sensors based on WO₃ nanorods decorated with Au nanoparticles, *Phys. E*, 2017, **90**, 109–115.

58 C.-S. Lee, I.-D. Kim and J.-H. Lee, Selective and sensitive detection of trimethylamine using ZnO–In₂O₃ composite nanofibers, *Sens. Actuators, B*, 2013, **181**, 463–470.

59 J. Rodrigues and N. G. Shimpi, Detection of trimethylamine (TMA) gas using mixed shape cobalt doped ZnO nanostructure, *Mater. Chem. Phys.*, 2023, **305**, 127972.

60 S. Ma, J. Guo, H. Zhang, X. Shao and D. Zhang, A Room Temperature Trimethylamine Gas Sensor Based on Electrospinned Molybdenum Oxide Nanofibers/Ti₃C₂Tx MXene Heterojunction, *Nanomaterials*, 2024, **14**(6), 537.

61 Z. Hu, X. Yang, Y. Zhang, Z. Sun, W. Liu, G. Pan, et al., High-performance trimethylamine gas sensor based on Sn-W co-doped MOF-derived hollow flower-like nickel oxide, *J. Alloys Compd.*, 2025, **1010**, 177110.

62 D. Meng, C. He, Y. Zhang, X. San, L. Zhang, Q. Jin, et al., Heterostructures constructed by NiMoO₄ functionalized 2D MoO₃ nanosheets for ultrasensitive trimethylamine detection with ppb level detection, *Sens. Actuators, B*, 2024, **421**, 136442.

63 S. Yang, H. Sun, Z. Sun, H. Wang and X. Yang, RuO₂ sensitized metal organic framework derived In₂O₃ hollow nanotubes for ultra-sensitive and high-humidity trimethylamine detection, *J. Alloys Compd.*, 2025, **1024**, 180255.

64 X. Sui, D. Zhang, J. Wang, M. Tang, H. Xia and Z. Wang, Ppb-level detection of trimethylamine as biomarker in exhaled gas based on MoO₃/V₂O₅ hierarchical heterostructure, *J. Alloys Compd.*, 2023, **968**, 172104.

65 Y. Ji, N. Zhang, J. Xu, Q. Jin, X. San and X. Wang, Co₃O₄/In₂O₃ pn heterostructures based gas sensor for efficient structure-driven trimethylamine detection, *Ceram. Int.*, 2023, **49**(11), 17354–17362.

66 Q. Xie, Y. Ding, Q. Wang and P. Song, Fabrication of 1D/2D In₂O₃ nanofibers/Ti₃C₂TX MXene composites for high performance detection of trimethylamine at low temperature, *Sens. Actuators, B*, 2024, **405**, 135338.

67 F. Wang, C. Wang, Z. Zhang, E. Liang, C. Yue, Z. Liu, et al., Selective trimethylamine sensors based on Co₃O₄ modified WO₃ spheres, *J. Alloys Compd.*, 2024, **1005**, 176254.

68 C. Zhao, J. Shen, S. Xu, J. Wei, H. Liu, S. Xie, et al., Ultra-efficient trimethylamine gas sensor based on Au nanoparticles sensitized WO₃ nanosheets for rapid assessment of seafood freshness, *Food Chem.*, 2022, **392**, 133318.

69 T. Yang, L. Du, C. Zhai, Z. Li, Q. Zhao, Y. Luo, et al., Ultrafast response and recovery trimethylamine sensor based on α-Fe₂O₃ snowflake-like hierarchical architectures, *J. Alloys Compd.*, 2017, **718**, 396–404.

70 P. Perillo and D. Rodríguez, Low temperature trimethylamine flexible gas sensor based on TiO₂ membrane nanotubes, *J. Alloys Compd.*, 2016, **657**, 765–769.

71 D. Meng, D. Liu, G. Wang, Y. Shen, X. San, J. Si, et al., In-situ growth of ordered Pd-doped ZnO nanorod arrays on ceramic tube with enhanced trimethylamine sensing performance, *Appl. Surf. Sci.*, 2019, **463**, 348–356.

72 H.-S. Woo, C. W. Na, I.-D. Kim and J.-H. Lee, Highly sensitive and selective trimethylamine sensor using one-dimensional ZnO–Cr₂O₃ hetero-nanostructures, *Nanotechnology*, 2012, **23**(24), 245501.

73 Z. Lou, F. Li, J. Deng, L. Wang and T. Zhang, Branch-like hierarchical heterostructure (α-Fe₂O₃/TiO₂): a novel sensing material for trimethylamine gas sensor, *ACS Appl. Mater. Interfaces*, 2013, **5**(23), 12310–12316.

74 X. Chu, S. Liang, T. Chen and Q. Zhang, Trimethylamine sensing properties of CdO–Fe₂O₃ nano-materials prepared using co-precipitation method in the presence of PEG400, *Mater. Chem. Phys.*, 2010, **123**(2), 396–400.

75 S.-H. Park, J.-Y. Ryu, H.-H. Choi and T.-H. Kwon, Zinc oxide thin film doped with Al₂O₃, TiO₂ and V₂O₅ as sensitive sensor for trimethylamine gas, *Sens. Actuators, B*, 1998, **46**(2), 75–79.

76 D. Meng, T. Qiao, G. Wang, Y. Shen, X. San, Y. Pan, et al., NiO-functionalized In₂O₃ flower-like structures with enhanced trimethylamine gas sensing performance, *Appl. Surf. Sci.*, 2022, **577**, 151877.

77 D. Meng, R. Li, G. Wang, Y. Zhang, X. San and X. Wang, Synthesis of NiMoO₄-functionalized MoO₃ nanorods with enhanced TMA gas sensing properties, *Sens. Actuators Rep.*, 2022, **4**, 100104.

78 C. Zheng, C. Zhang, L. He, K. Zhang, J. Zhang, L. Jin, et al., ZnFe2O4/ZnO nanosheets assembled microspheres for high performance trimethylamine gas sensing, J. Alloys Compd., 2020, 849, 156461.

79 Y. Li, K. Li, Y. Luo, B. Liu, H. Wang, L. Gao, et al., Synthesis of Co3O4/ZnO nano-heterojunctions by one-off processing ZIF-8@ ZIF-67 and their gas-sensing performances for trimethylamine, Sens. Actuators, B, 2020, 308, 127657.

80 D. Zappa, A. Bertuna, E. Comini, N. Kaur, N. Poli, V. Sberveglieri, et al., Metal oxide nanostructures: preparation, characterization and functional applications as chemical sensors, Beilstein J. Nanotechnol., 2017, 8(1), 1205–1217.

81 A. Singh, S. Sikarwar, A. Verma and B. Chandra Yadav, The recent development of metal oxide heterostructures based gas sensor, their future opportunities and challenges: A review, Sens. Actuators, A, 2021, 332, 113127.

82 K. Wu, M. Debliquy and C. Zhang, Metal–oxide–semiconductor resistive gas sensors for fish freshness detection, Compr. Rev. Food Sci. Food Saf., 2023, 22(2), 913–945.

83 S. Gbadamasi, M. Mohiuddin, V. Krishnamurthi, R. Verma, M. W. Khan, S. Pathak, et al., Interface chemistry of two-dimensional heterostructures–fundamentals to applications, Chem. Soc. Rev., 2021, 50(7), 4684–4729.

84 T. A. Shifa, F. Wang, Y. Liu and J. He, Heterostructures based on 2D materials: a versatile platform for efficient catalysis, Adv. Mater., 2019, 31(45), 1804828.

85 J. Guo, R. Xiang, T. Cheng, S. Maruyama and Y. Li, One-dimensional van der Waals heterostructures: A perspective, ACS Nanosci. Au, 2021, 2(1), 3–11.

86 Y. Zhong, C. Peng, Z. He, D. Chen, H. Jia, J. Zhang, et al., Interface engineering of heterojunction photocatalysts based on 1D nanomaterials, Catal. Sci. Technol., 2021, 11(1), 27–42.

87 J.-Y. Li, L. Yuan, S.-H. Li, Z.-R. Tang and Y.-J. Xu, One-dimensional copper-based heterostructures toward photo-driven reduction of CO 2 to sustainable fuels and feedstocks, J. Mater. Chem. A, 2019, 7(15), 8676–8689.

88 N. Rahman, J. Yang, M. Sohail, R. Khan, A. Iqbal, C. Maouche, et al., Insight into metallic oxide semiconductor (SnO2, ZnO, CuO, α-Fe2O3, WO3)-carbon nitride (g-C3N4) heterojunction for gas sensing application, Sens. Actuators, A, 2021, 332, 113128.

89 J. Gao, K. Wang, J. Cao, M. Zhang, F. Lin, M. Ling, et al., Recent Progress of Self-Supported Metal Oxide Nano-Porous Arrays in Energy Storage Applications, Small, 2023, 19(45), 2302786.

90 M. Santucci, M. L. Ermini, G. Bresciani, A. Griesi, M. Gemmi, G. Pampaloni, et al., Total-and semi-bare noble metal nanoparticles@ silica core@ shell catalysts for hydrogen generation by formic acid decomposition, Emergent Mater., 2021, 4, 483–491.

91 C. Lamiel, I. Hussain, O. R. Ogunsakin and K. Zhang, MXene in core–shell structures: research progress and future prospects, J. Mater. Chem. A, 2022, 10(27), 14247–14272.

92 W. Guan, N. Tang, K. He, X. Hu, M. Li and K. Li, Gas-sensing performances of metal oxide nanostructures for detecting dissolved gases: a mini review, Front. Chem., 2020, 8, 76.

93 T. Lin, X. Lv, S. Li and Q. Wang, The morphologies of the semiconductor oxides and their gas-sensing properties, Sensors, 2017, 17(12), 2779.

94 A. Foroozandeh, H. SalarAmoli, M. Abdouss and M. Pourmadadi, Development of a labeled-free and labeled electrochemical aptasensor for the detection of cancer antigen 125 by using magnetic g-C3N4/MoS2 nanocomposite, Sens. Actuators Rep., 2024, 7, 100195.

95 S. P. Borderud, Y. Li, J. E. Burkhalter, C. E. Sheffer and J. S. Ostroff, Electronic cigarette use among patients with cancer: characteristics of electronic cigarette users and their smoking cessation outcomes, Cancer, 2014, 120(22), 3527–3535.

96 R. Paul, B. Das and R. Ghosh, Novel approaches towards design of metal oxide based hetero-structures for room temperature gas sensor and its sensing mechanism: A recent progress, J. Alloys Compd., 2023, 941, 168943.

97 A. Bag and N.-E. Lee, Gas sensing with heterostructures based on two-dimensional nanostructured materials: a review, J. Mater. Chem. C, 2019, 7(43), 13367–13383.

98 S. Aftab, M. Z. Iqbal, S. Hussain, H. H. Hegazy, F. Kabir, S. H. A. Jaffery, et al., New developments in gas sensing using various two-dimensional architectural designs, Chem. Eng. J., 2023, 469, 144039.

99 Z. Jin, M. Xiao, Z. Bao, P. Wang and J. Wang, A general approach to mesoporous metal oxide microspheres loaded with noble metal nanoparticles, Angew. Chem., Int. Ed. Engl., 2012, 51(26), 6406–6410.

100 J. M. Walker, S. A. Akbar and P. A. Morris, Synergistic effects in gas sensing semiconducting oxide nano-heterostructures: A review, Sens. Actuators, B, 2019, 286, 624–640.

101 Z. Li, H. Li, Z. Wu, M. Wang, J. Luo, H. Torun, et al., Advances in designs and mechanisms of semiconducting metal oxide nanostructures for high-precision gas sensors operated at room temperature, Mater. Horiz., 2019, 6(3), 470–506.

102 W. Raza, A. Shaheen, N. A. Khan, K. H. Kim and X. Cai, Advanced strategies for the synthesis and modulation of 2D layered heterostructures for energy conversion and storage applications, Prog. Mater. Sci., 2024, 101325.

103 Y. L. Shi, Q. Lv, Y. C. Tao, Y. X. Ma and X. D. Wang, Design and growth of branched organic crystals: recent advances and future applications, Angew. Chem., 2022, 134(40), e202208768.

104 R. Ghosh and P. K. Giri, Silicon nanowire heterostructures for advanced energy and environmental applications: a review, Nanotechnology, 2016, 28(1), 012001.

105 M. W. Alam, P. Pooja, M. Aamir, B. Souayeh, S. Mushtaq, M. S. Khan, et al., The recent development in chemoresistive-based heterostructure gas sensor technology, their future opportunities and challenges: A review, Membranes, 2022, 12(6), 555.

106 N. Kaur, M. Singh and E. Comini, Materials engineering strategies to control metal oxides nanowires sensing properties, *Adv. Mater. Interfaces*, 2022, **9**(12), 2101629.

107 F. Caruso, R. A. Caruso and H. Mohwald, Nanoengineering of inorganic and hybrid hollow spheres by colloidal templating, *Science*, 1998, **282**(5391), 1111–1114.

108 Y. Liu, S. Xiao and K. Du, Chemiresistive gas sensors based on hollow heterojunction: A review, *Adv. Mater. Interfaces*, 2021, **8**(12), 2002122.

109 M. Zhu, Y. Cheng, Q. Luo, M. El-khateeb and Q. Zhang, A review of synthetic approaches to hollow nanostructures, *Mater. Chem. Front.*, 2021, **5**(6), 2552–2587.

110 Y. Li, J. Liu, D. J. McClements, X. Zhang, T. Zhang and Z. Du, Recent advances in Hollow nanostructures: synthesis methods, structural characteristics, and applications in Food and Biomedicine, *J. Agric. Food Chem.*, 2024, **72**(37), 20241–20260.

111 Y. Xu, T. Ma, L. Zheng, Y. Zhao, X. Liu and J. Zhang, Heterostructures of hematite-sensitized W18O49 hollow spheres for improved acetone detection with ultralow detection limit, *Sens. Actuators, B*, 2019, **288**, 432–441.

112 K.-M. Kim, K.-I. Choi, H.-M. Jeong, H.-J. Kim, H.-R. Kim and J.-H. Lee, Highly sensitive and selective trimethylamine sensors using Ru-doped SnO2 hollow spheres, *Sens. Actuators, B*, 2012, **166–167**, 733–738.

113 R. Xavier and K. Sivaperuman, Review on the of physical vapor deposition on imminent chemiresistive metal oxide gas sensors and their future scope, *Mater. Today Commun.*, 2024, **38**, 107831.

114 J. Tan, S. Li, B. Liu and H.-M. Cheng, Structure, preparation, and applications of 2D material-based metal–semiconductor heterostructures, *Small Struct.*, 2021, **2**(1), 2000093.

115 Y. Liu, H. Ma, X. X. Han and B. Zhao, Metal–semiconductor heterostructures for surface-enhanced Raman scattering: synergistic contribution of plasmons and charge transfer, *Mater. Horiz.*, 2021, **8**(2), 370–382.

116 P. Wang, C. Jia, Y. Huang and X. Duan, Van der Waals heterostructures by design: from 1D and 2D to 3D, *Matter*, 2021, **4**(2), 552–581.

117 N. Rajamanickam, S. Kanmani and K. Ramachandran, Synthesis of heterostructure metal oxide nanocomposites and their gas-sensing properties, *Complex and Composite Metal Oxides for Gas, VOC and Humidity Sensors*, 2024, vol. 2, pp. 27–59.

118 S. Joseph, J. Mohan, S. Lakshmy, S. Thomas, B. Chakraborty, S. Thomas, *et al.*, A review of the synthesis, properties, and applications of 2D transition metal dichalcogenides and their heterostructures, *Mater. Chem. Phys.*, 2023, **297**, 127332.

119 R. Wu, J. Hao and Y. Wang, Recent Advances in Engineering of 2D Layered Metal Chalcogenides for Resistive-Type Gas Sensor, *Small*, 2024, **20**(49), 2404821.

120 S. Pei, Z. Wang and J. Xia, High pressure studies of 2D materials and heterostructures: A review, *Mater. Des.*, 2022, **213**, 110363.

121 S. Shah, S. Hussain, S. T. U. Din, A. Shahid, J. N. O. Amu-Darko, M. Wang, *et al.*, A Review on In2O3 Nanostructures for Gas Sensing Applications, *J. Environ. Chem. Eng.*, 2024, 112538.

122 P. Raju and Q. Li, Semiconductor materials and devices for gas sensors, *J. Electrochem. Soc.*, 2022, **169**(5), 057518.

123 V. Khoramshahi, M. Azarang, M. Nouri, A. Shirmardi and R. Yousefi, Metal oxide/g-C3N4 nanocomposites chemiresistive gas sensors: A review on enhanced performance, *Talanta Open*, 2024, 100290.

124 T. Zhou and T. Zhang, Insights into the gas sensor materials: Synthesis, performances and devices, *Sens. Actuators, B*, 2022, **371**, 132565.

125 S. Das, S. Mojumder, D. Saha and M. Pal, Influence of major parameters on the sensing mechanism of semiconductor metal oxide based chemiresistive gas sensors: A review focused on personalized healthcare, *Sens. Actuators, B*, 2022, **352**, 131066.

126 H.-J. Kim and J.-H. Lee, Highly sensitive and selective gas sensors using p-type oxide semiconductors: Overview, *Sens. Actuators, B*, 2014, **192**, 607–627.

127 S. A. Müller, D. Degler, C. Feldmann, M. Türk, R. Moos, K. Fink, *et al.*, Exploiting synergies in catalysis and gas sensing using noble metal-loaded oxide composites, *ChemCatChem*, 2018, **10**(5), 864–880.

128 F. E. Ab Latif, A. Numan, N. M. Mubarak, M. Khalid, E. C. Abdullah, N. A. Manaf, *et al.*, Evolution of MXene and its 2D heterostructure in electrochemical sensor applications, *Coord. Chem. Rev.*, 2022, **471**, 214755.

129 M. Hübner, C. E. Simion, A. Tomescu-Stănoiu, S. Pokhrel, N. Bârsan and U. Weimar, Influence of humidity on CO sensing with p-type CuO thick film gas sensors, *Sens. Actuators, B*, 2011, **153**(2), 347–353.

130 J. C. Védrine, Heterogeneous catalysis on metal oxides, *Catalysts*, 2017, **7**(11), 341.

131 L. Li, A. Wang, B. Qiao, J. Lin, Y. Huang, X. Wang, *et al.*, Origin of the high activity of Au/FeOx for low-temperature CO oxidation: Direct evidence for a redox mechanism, *J. Catal.*, 2013, **299**, 90–100.

132 X. Y. Liu, A. Wang, T. Zhang and C.-Y. Mou, Catalysis by gold: New insights into the support effect, *Nano Today*, 2013, **8**(4), 403–416.

133 A. Mirzaei, J. H. Bang, S. S. Kim and H. W. Kim, Effect of noble metals on hydrogen sensing properties of metal oxide-based gas sensors, *J. Sens. Sci. Technol.*, 2020, **29**(6), 365–368.

134 P. T. Moseley, Progress in the development of semiconducting metal oxide gas sensors: A review, *Meas. Sci. Technol.*, 2017, **28**(8), 082001.

135 D. Zhang, C. Jiang and Y. Zhang, Room temperature hydrogen gas sensor based on palladium decorated tin oxide/molybdenum disulfide ternary hybrid via hydrothermal route, *Sens. Actuators, B*, 2017, **242**, 15–24.

136 J. Hu, Y. Zou, Y. Deng, H.-J. Li, H. Xu, D. Wang, *et al.*, Recent advances in non-ionic surfactant templated synthesis of porous metal oxide semiconductors for gas sensing applications, *Prog. Mater. Sci.*, 2024, 101409.

137 J. Xu, X. He, K. Xu, H. Liao and C. Zhang, Synthesis and optimization strategies of nanostructured metal oxides for chemiresistive methanol sensors, *Ceram. Int.*, 2023, **49**(13), 21113–21132.

138 X. Tian, L. Yao, X. Cui, R. Zhao, T. Chen, X. Xiao, *et al.*, A two-dimensional Ti 3 C 2 TX MXene@ TiO 2/MoS 2 heterostructure with excellent selectivity for the room temperature detection of ammonia, *J. Mater. Chem. A*, 2022, **10**(10), 5505–5519.

139 H. Ma, L. Yu, X. Yuan, Y. Li, C. Li, M. Yin, *et al.*, Room temperature photoelectric NO2 gas sensor based on direct growth of walnut-like In2O3 nanostructures, *J. Alloys Compd.*, 2019, **782**, 1121–1126.

140 Y. Tie, S. Y. Ma, S. T. Pei, K. M. Zhu, Q. X. Zhang, R. Zhang, *et al.*, Formaldehyde sensing characteristics of hydrothermally synthesized Zn2SnO4 nanocubes, *Mater. Lett.*, 2020, **259**, 126896.

141 Y. Ji, N. Zhang, J. Xu, Q. Jin, X. San and X. Wang, Co3O4/In2O3 p–n heterostructures based gas sensor for efficient structure-driven trimethylamine detection, *Ceram. Int.*, 2023, **49**(11, Part A), 17354–17362.

142 Y. Ren, Y. Zou, Y. Liu, X. Zhou, J. Ma, D. Zhao, *et al.*, Synthesis of orthogonally assembled 3D cross-stacked metal oxide semiconducting nanowires, *Nat. Mater.*, 2020, **19**(2), 203–211.

143 Z. Li, Y. Zhang, H. Zhang, Y. Jiang and J. Yi, Superior NO2 Sensing of MOF-Derived Indium-Doped ZnO Porous Hollow Cages, *ACS Appl. Mater. Interfaces*, 2020, **12**(33), 37489–37498.

144 L. Zhu, J. Wang, J. Liu, X. Chen, Z. Xu, Q. Ma, *et al.*, Designing highly sensitive formaldehyde sensors via A-site cation deficiency in LaFeO3 hollow nanofibers, *Appl. Surf. Sci.*, 2022, **590**, 153085.

145 J. Xu and C. Zhang, Oxygen vacancy engineering on cerium oxide nanowires for room-temperature linalool detection in rice aging, *J. Adv. Ceram.*, 2022, **11**(10), 1559–1570.

146 H. Liu, H. Zhang, W. Zhu, M. Bo and T. Zhao, Crystalline-to-Amorphous Phase Transformation in CuO Nanowires for Gaseous Ionization and Sensing Application, *ACS Sens.*, 2021, **6**(11), 4118–4125.

147 P. Yang, Y. Fan, K. Hu, L. Jiang, L. Tan, Z. Wang, *et al.*, Fast, Sensitive, and Highly Selective Room-Temperature Hydrogen Sensing of Defect-Rich Orthorhombic Nb2O5–x Nanobelts with an Abnormal p-Type Sensor Response, *ACS Appl. Mater. Interfaces*, 2022, **14**(22), 25937–25948.

148 A. Keirouz, Z. Wang, V. S. Reddy, Z. K. Nagy, P. Vass, M. Buzgo, *et al.*, The history of electrospinning: Past, present, and future developments, *Adv. Mater. Technol.*, 2023, **8**(11), 2201723.

149 M. Rahmati, D. K. Mills, A. M. Urbanska, M. R. Saeb, J. R. Venugopal, S. Ramakrishna, *et al.*, Electrospinning for tissue engineering applications, *Prog. Mater. Sci.*, 2021, **117**, 100721.

150 F. Meng, Z. Liao, C. Xing, Z. Yuan, R. Zhang, H. Zhu, *et al.*, Preparation of SnO2/SiO2 nanocomposites by sol-gel method for enhancing the gas sensing performance to triethylamine, *J. Alloys Compd.*, 2022, **893**, 162189.

151 M. O. Mavukkandy, S. A. McBride, D. M. Warsinger, N. Dizge, S. W. Hasan and H. A. Arafat, Thin film deposition techniques for polymeric membranes– A review, *J. Membr. Sci.*, 2020, **610**, 118258.

152 S. Obregón and V. Rodríguez-González, Photocatalytic TiO 2 thin films and coatings prepared by sol–gel processing: A brief review, *J. Sol-Gel Sci. Technol.*, 2021, 1–17.

153 M. Parashar, V. K. Shukla and R. Singh, Metal oxides nanoparticles via sol–gel method: a review on synthesis, characterization and applications, *J. Mater. Sci.: Mater. Electron.*, 2020, **31**(5), 3729–3749.

154 D. Bokov, A. Turki Jalil, S. Chupradit, W. Suksatan, M. Javed Ansari, I. H. Shewael, *et al.*, Nanomaterial by sol-gel method: synthesis and application, *Adv. Mater. Sci. Eng.*, 2021, **2021**(1), 5102014.

155 E. Benrezgua, B. Deghfel, A. Mahroug, M. K. Yaakob, A. Boukhari, R. Amari, *et al.*, Experimental and theoretical studies on structural, morphological, electronic, optical and magnetic properties of Zn1-xCuxO thin films (0≤x≤0.125), *Mater. Sci. Semicond. Process.*, 2021, **134**, 106012.

156 H. Maleki, M.-A. Shahbazi, S. Montes, S. H. Hosseini, M. R. Eskandari, S. Zaunschirm, *et al.*, Mechanically strong silica-silk fibroin bioaerogel: a hybrid scaffold with ordered honeycomb micromorphology and multiscale porosity for bone regeneration, *ACS Appl. Mater. Interfaces*, 2019, **11**(19), 17256–17269.

157 S. Ahmad, S. Ahmad and J. N. Sheikh, Silica centered aerogels as advanced functional material and their applications: A review, *J. Non-Cryst. Solids*, 2023, **611**, 122322.

158 J. K. Rajput, T. K. Pathak, V. Kumar, H. Swart and L. Purohit, Controlled sol–gel synthesis of oxygen sensing CdO: ZnO hexagonal particles for different annealing temperatures, *RSC Adv.*, 2019, **9**(54), 31316–31324.

159 S. Lee, S. Kim, G. B. Nam, T. H. Eom and H. W. Jang, Chemoresistive Gas Sensors for Food Quality Monitoring, *J. Semicond. Technol. Sci.*, 2022, **22**(4), 244–258.

160 B. Nadekar, Y. B. Khollam, S. F. Shaikh, A. Trimukhe, R. Deshmukh, P. S. More, *et al.*, Plasma-Polymerized thiophene-reduced graphene oxide composite film sensor for ammonia/amine detection at room temperature, *Chemosensors*, 2023, **11**(1), 42.

161 A. Foroozandeh, P. Hatefirad, Z. Safaei Mahmoudabadi and A. Tavasoli, Catalytic activity of synthesized NiMo catalysts on walnut shell activated carbon for heavy naphtha hydrotreating, *Iran. J. Chem. Chem. Eng.*, 2023, **42**(1), 38–50.

162 T. Hu, X. Chu, F. Gao, Y. Dong, W. Sun and L. Bai, Trimethylamine sensing properties of graphene quantum Dots/α-Fe2O3 composites, *J. Solid State Chem.*, 2016, **237**, 284–291.

163 B. Mahata, S. Giri, P. Banerji and P. K. Guha, Cactus-Like NiO Nanostructure-Based ppb Level Trimethylamine Gas Sensor for Monitoring Saltwater Fish Freshness, *ACS Food Sci. Technol.*, 2024, **5**(1), 284–291.

164 W. Sun, J. Li, H. Li, B. Jin, Z. Li, T. Zhang, *et al.*, Mechanistic insights into ball milling enhanced montmorillonite

modification with tetramethylammonium for adsorption of gaseous toluene, *Chemosphere*, 2022, **296**, 133962.

165 Y.-L. Sun, W. Jevasuwan and N. Fukata, Top-down fabrication of Si nanotube arrays using nanoimprint lithography and spacer patterning for electronic and optoelectronic applications, *Mater. Today Nano*, 2024, **28**, 100547.

166 J. Zhao, N. Yi, X. Ding, S. Liu, J. Zhu, A. C. Castonguay, *et al.*, In situ laser-assisted synthesis and patterning of graphene foam composites as a flexible gas sensing platform, *Chem. Eng. J.*, 2023, **456**, 140956.

167 V. Karthikeyan, A. Suganthi, P. A. Jose, C. Gopi, S. Ponsadailakshmi, N. Moorthy, *et al.*, Tuning the cathode power to Deposit Amphoteric Vanadia as a dimethylamine sensor at room temperature, *Mater. Lett.*, 2025, **381**, 137800.

168 N. Yamazoe, G. Sakai and K. Shimanoe, Oxide semiconductor gas sensors, *Catal. Surv. Asia*, 2003, **7**, 63–75.

169 G. Neri, First Fifty Years of Chemoresistive Gas Sensors, *Chemosensors*, 2015, **3**(1), 1–20.

170 S. Park, G.-J. Sun, C. Jin, H. W. Kim, S. Lee and C. Lee, Synergistic effects of a combination of Cr2O3-functionalization and UV-irradiation techniques on the ethanol gas sensing performance of ZnO nanorod gas sensors, *ACS Appl. Mater. Interfaces*, 2016, **8**(4), 2805–2811.

171 S. Park, G.-J. Sun, H. Kheel, W. I. Lee, S. Lee, S.-B. Choi, *et al.*, Synergistic effects of codecoration of oxide nanoparticles on the gas sensing performance of In2O3 nanorods, *Sens. Actuators, B*, 2016, **227**, 591–599.

172 J.-H. Kim, H.-M. Jeong, C. W. Na, J.-W. Yoon, F. Abdel-Hady, A. Wazzan, *et al.*, Highly selective and sensitive xylene sensors using Cr2O3-ZnCr2O4 hetero-nanostructures prepared by galvanic replacement, *Sens. Actuators, B*, 2016, **235**, 498–506.

173 E. Comini, C. Baratto, I. Concina, G. Faglia, M. Falasconi, M. Ferroni, *et al.*, Metal oxide nanoscience and nanotechnology for chemical sensors, *Sens. Actuators, B*, 2013, **179**, 3–20.

174 A. Dey, Semiconductor metal oxide gas sensors: A review, *Mater. Sci. Eng., B*, 2018, **229**, 206–217.

175 N. Hongsith, C. Viriyaworasakul, P. Mangkorntong, N. Mangkorntong and S. Choopun, Ethanol sensor based on ZnO and Au-doped ZnO nanowires, *Ceram. Int.*, 2008, **34**(4), 823–826.

176 N. Kaur, E. Comini, D. Zappa, N. Poli and G. Sberveglieri, Nickel oxide nanowires: Vapor liquid solid synthesis and integration into a gas sensing device, *Nanotechnology*, 2016, **27**(20), 205701.

177 D. MENGa, E. Comini and G. Sberveglieri, Thermally oxidized zinc oxide nanowires for use as chemical sensors, *Nanotechnology*, 2013, **24**(44), 444008.

178 N. Kaur, E. Comini, N. Poli, D. Zappa and G. Sberveglieri, NiO/ZnO nanowire-heterostructures by vapor phase growth for gas sensing, *Procedia Eng.*, 2016, **168**, 1140–1143.

179 E. Comini, C. Baratto, G. Faglia, M. Ferroni, A. Vomiero and G. Sberveglieri, Quasi-one dimensional metal oxide

semiconductors: Preparation, characterization and application as chemical sensors, *Prog. Mater. Sci.*, 2009, **54**(1), 1–67.

180 D. R. Miller, S. A. Akbar and P. A. Morris, Nanoscale metal oxide-based heterojunctions for gas sensing: A review, *Sens. Actuators, B*, 2014, **204**, 250–272.

181 L.-Y. Gai, R.-P. Lai, X.-H. Dong, X. Wu, Q.-T. Luan, J. Wang, *et al.*, Recent advances in ethanol gas sensors based on metal oxide semiconductor heterojunctions, *Rare Met.*, 2022, **41**(6), 1818–1842.

182 Z. Wang, L. Zhu, S. Sun, J. Wang and W. Yan, One-dimensional nanomaterials in resistive gas sensor: From material design to application, *Chemosensors*, 2021, **9**(8), 198.

183 T. Lin, X. Lv, Z. Hu, A. Xu and C. Feng, Semiconductor metal oxides as chemoresistive sensors for detecting volatile organic compounds, *Sensors*, 2019, **19**(2), 233.

184 A. Mirzaei, J.-H. Lee, S. M. Majhi, M. Weber, M. Bechelany and H. W. Kim, Resistive gas sensors based on metal-oxide nanowires, *J. Appl. Phys.*, 2019, **126**(24), 241102.

185 T. Li, W. Zeng and Z. Wang, Quasi-one-dimensional metal-oxide-based heterostructural gas-sensing materials: A review, *Sens. Actuators, B*, 2015, **221**, 1570–1585.

186 D. Xue, J. Wang, Y. Wang, G. Sun, J. Cao, H. Bala, *et al.*, Enhanced Methane Sensing Properties of WO3 Nanosheets with Dominant Exposed (200) Facet via Loading of SnO2 Nanoparticles, *Nanomaterials*, 2019, **9**(3), 351.

187 X. Li, J. H. Cho, P. Kurup and Z. Gu, Novel sensor array based on doped tin oxide nanowires for organic vapor detection, *Sens. Actuators, B*, 2012, **162**(1), 251–258.

188 S. Kaaliveetil, J. Yang, S. Alssaidy, Z. Li, Y. Cheng, N. Menon, *et al.*, Microfluidic Gas Sensors: Detection Principle and Applications, *Micromachines*, 2022, **13**, 1716.

189 M. Ghazi, N. Tasnim and M. Hoorfar, Selective monitoring of natural gas sulphur-based odorant mixture of t-butyl mercaptan and methyl ethyl sulphide using an array of microfluidic gas sensors, *J. Hazard. Mater.*, 2022, **438**, 129548.

190 V. Martini, S. Bernardini, M. Bendahan, K. Aguir, P. Perrier and I. Graur, Microfluidic gas sensor with integrated pumping system, *Sens. Actuators, B*, 2012, **170**, 45–50.

191 Y. Xing and P. S. Dittrich, One-dimensional nanostructures: Microfluidic-based synthesis, alignment and integration towards functional sensing devices, *Sensors*, 2018, **18**(1), 134.

192 P. Bindra and A. Hazra, Selective detection of organic vapors using TiO2 nanotubes based single sensor at room temperature, *Sens. Actuators, B*, 2019, **290**, 684–690.

193 S. Kaaliveetil, Y.-Y. Lee, Z. Li, Y.-H. Cheng, N. H. Menon, S. Dongare, *et al.*, Ionic Liquid-Packed Microfluidic Device with Non-Planar Microelectrode as a Miniaturized Electrochemical Gas Sensor, *J. Electrochem. Soc.*, 2023, **170**(8), 087508.

194 X. Zhang, Z. Zhu, N. Xiang and Z. Ni, A microfluidic gas damper for stabilizing gas pressure in portable microfluidic systems, *Biomicrofluidics*, 2016, **10**(5), 054123.

195 R. S. Andre, L. A. Mercante, M. H. Facure, R. C. Sanfelice, L. Fugikawa-Santos, T. M. Swager, *et al.*, Recent progress in amine gas sensors for food quality monitoring: novel architectures for sensing materials and systems, *ACS Sens.*, 2022, **7**(8), 2104–2131.

196 M. Paknahad, J. S. Bachhal, A. Ahmadi and M. Hoorfar, Characterization of channel coating and dimensions of microfluidic-based gas detectors, *Sens. Actuators, B*, 2017, **241**, 55–64.

197 M. N. Madhubhashini, C. P. Liyanage, A. U. Alahakoon and R. P. Liyanage, Current applications and future trends of artificial senses in fish freshness determination: A review, *J. Food Sci.*, 2024, **89**(1), 33–50.

198 R. Saeed, H. Feng, X. Wang, X. Zhang and Z. Fu, Fish quality evaluation by sensor and machine learning: A mechanistic review, *Food Control*, 2022, **137**, 108902.

199 A. Degas, M. R. Islam, C. Hurter, S. Barua, H. Rahman, M. Poudel, *et al.*, A survey on artificial intelligence (ai) and explainable ai in air traffic management: Current trends and development with future research trajectory, *Appl. Sci.*, 2022, **12**(3), 1295.

200 C. Bilgera, A. Yamamoto, M. Sawano, H. Matsukura and H. Ishida, Application of convolutional long short-term memory neural networks to signals collected from a sensor network for autonomous gas source localization in outdoor environments, *Sensors*, 2018, **18**(12), 4484.

201 X. Pan, H. Zhang, W. Ye, A. Bermak and X. Zhao, A fast and robust gas recognition algorithm based on hybrid convolutional and recurrent neural network, *IEEE Access*, 2019, **7**, 100954–100963.

202 Q. Liu, X. Hu, M. Ye, X. Cheng and F. Li, Gas recognition under sensor drift by using deep learning, *Int. J. Intell. Syst.*, 2015, **30**(8), 907–922.

203 S. Hamilton and B. Charalambous, *Leak Detection: Technology and Implementation*, IWA Publishing, 2013.

204 *Leveraging Drone Based Imaging Technology for Pipeline and RoU Monitoring Survey. SPE Asia Pacific Health, Safety, Security, Environment and Social Responsibility Symposium?*, ed. Marathe S., SPE, 2019.

205 *Gas Leakage Detection Using Thermal Imaging Technique. 2014 UKSim-AMSS 16th International Conference on Computer Modelling and Simulation*, ed. Jadin M. S. and Ghazali K. H., IEEE, 2014.

206 An artificial intelligence enabled smart industrial automation system based on internet of things assistance, *2022 International Conference on Advances in Computing, Communication and Applied Informatics (ACCAI)*, ed. Nirmala P., Ramesh S., Tamilselvi M., Ramkumar G. and Anitha G., IEEE, 2022.

207 N. X. Thai, M. Tonezzer, L. Masera, H. Nguyen, N. Van Duy and N. D. Hoa, Multi gas sensors using one nanomaterial, temperature gradient, and machine learning algorithms for discrimination of gases and their concentration, *Anal. Chim. Acta*, 2020, **1124**, 85–93.

208 H. Mei, J. Peng, T. Wang, T. Zhou, H. Zhao, T. Zhang, *et al.*, Overcoming the limits of cross-sensitivity: pattern recognition methods for chemiresistive gas sensor array, *Nano-Micro Lett.*, 2024, **16**(1), 269.

209 V. Mohammadi and S. Minaei, Artificial intelligence in the production process, *Engineering Tools in the Beverage Industry*, Elsevier, 2019, pp. 27–63.

210 M. Chowdhury and M. Oehlschlaeger, Artificial Intelligence in Gas Sensing: A Review, *ACS Sens.*, 2025, **10**(3), 1538–1563.

211 M. Ghazi, S. Janfaza, H. Tahmooressi, A. Ravishankara, E. Earl, N. Tasnim, *et al.*, Enhanced selectivity of microfluidic gas sensors by modifying microchannel geometry and surface chemistry with graphene quantum dots, *Sens. Actuators, B*, 2021, **342**, 130050.

212 M. Aghaseyedi, A. Salehi, S. Valijam and M. Shooshtari, Gas selectivity enhancement using serpentine microchannel shaped with optimum dimensions in microfluidic-based gas sensor, *Micromachines*, 2022, **13**(9), 1504.

213 M. M. Montazeri, A. O'Brien and M. Hoorfar, Understanding microfluidic-based gas detectors: A numerical model to investigate fundamental sensor operation, influencing phenomena and optimum geometries, *Sens. Actuators, B*, 2019, **300**, 126904.

214 T. Wang, S. Ma, A. Lv, F. Liu and X. Yin, Concentration recognition of gas sensor with organic field-effect transistor assisted by artificial intelligence, *Sens. Actuators, B*, 2022, **363**, 131854.

215 U. Yaqoob and M. I. Younis, Chemical gas sensors: Recent developments, challenges, and the potential of machine learning—A review, *Sensors*, 2021, **21**(8), 2877.

216 Z. Chen, Z. Chen, Z. Song, W. Ye and Z. Fan, Smart gas sensor arrays powered by artificial intelligence, *J. Semicond.*, 2019, **40**(11), 111601.